

**Fig. 4.12.** The excited state  $e$  of the centre  $A$  lies in the conduction band of the host lattice. Photo-excitation of  $A$  (arrow) may be followed by photoionization

is strongly changed or even completely quenched by photoionization. The principle is illustrated in Figure 4.12. The luminescent center  $A$  has its ground state in the forbidden zone between valence and conduction bands. Its excited state lies in the conduction band. This implies that in the excited state an electron can easily be ionized from the center to the conduction band. It may recombine nonradiatively with a hole somewhere else, so that the luminescence is quenched. On the other hand the electron in the conduction band and the hole on the ionized centre will attract each other and may form an exciton. Since this exciton is bound to the luminescent center, radiative recombination of this exciton is known as impurity-bound exciton recombination [14]. However, the recombination may also be nonradiative.

A nice example is the isostructural series  $\text{CaF}_2 : \text{Yb}^{2+}$ ,  $\text{SrF}_2 : \text{Yb}^{2+}$  and  $\text{BaF}_2 : \text{Yb}^{2+}$  [14]. The calcium compound shows normal  $\text{Yb}^{2+}$  emission (Sect. 3.3.3), the strontium compound shows a strikingly different emission, viz. impurity-bound exciton emission, and the barium compound does not show any emission at all. Obviously the  $\text{Yb}^{2+}$  energy level scheme moves upwards in the energy band picture of the host lattice going from  $\text{CaF}_2$  to  $\text{BaF}_2$ .

Also  $\text{BaF}_2 : \text{Eu}^{2+}$  does not show  $\text{Eu}^{2+}$  emission, but impurity-bound exciton emission. The same holds for  $\text{NaF} : \text{Cu}^+$  where the excited state consists of a Jahn-Teller distorted  $\text{Cu}^{2+}$  ion which binds an electron. The absence of luminescence in  $\text{La}_2\text{O}_3 : \text{Ce}^{3+}$  has also been ascribed to quenching by photoionization [15].

Closely related to photoionization and its consequences is quenching of luminescence by electron transfer. This process is well known in coordination chemistry, but has been overlooked in solid state studies. The principle is outlined in Figure 4.13 for a system of two species,  $A$  and  $B$ . The first excited state is one in which only  $A$  is excited ( $A^* + B$ ). At higher energies we find a charge-transfer state  $A^+ + B^-$  with a large offset. Although  $A^+ + B^-$  lies at higher energy than  $A^* + B$ , judging from the absorption spectrum, the luminescence  $A^* \rightarrow A$  is quenched via the charge-transfer state.

This implies that a combination of a center which has a tendency to become oxidized with a center which has a tendency to become reduced will probably not show efficient luminescence. This is illustrated by some examples:

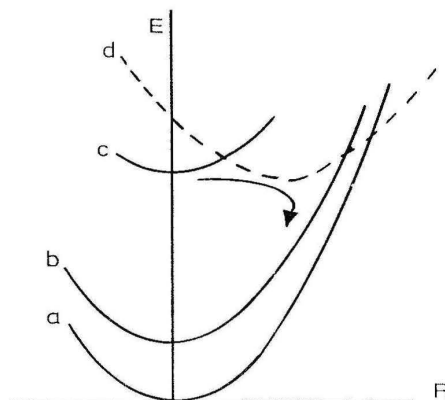


**Fig. 4.13.** Luminescence quenching by electron transfer. The ground state  $a$  consists of two species,  $A + B$ . In the excited states  $b$  and  $c$  the  $A$  ion is excited:  $A^* + B$ . State  $d$  is the electron-transfer state  $A^+ + B^-$ . Luminescence from the level  $c$  is quenched by electron transfer as indicated by the arrow

- whereas many rare earth ions show efficient luminescence in  $YVO_4$ , the ions  $Ce^{3+}$ ,  $Pr^{3+}$  and  $Tb^{3+}$  do not. This is due to quenching via a charge-transfer state ( $RE^{4+} + V^{4+}$ ) which is at low energy for these three ions and at much higher energy for the others.
- whereas many rare earth ions show efficient luminescence in cerium compounds,  $Eu^{3+}$  does not. Quenching occurs via a charge-transfer state ( $Ce^{4+} + Eu^{2+}$ ) which is at low energy. Further examples are given in Ref. [16].

Note that quenching by electron transfer is a special case of quenching via a charge-transfer state as discussed above (Sect. 4.2.2) for  $Eu^{3+}$ . There is also no principal difference between quenching by electron transfer and quenching via photoionization. However, the former has a localized character, the latter is used in energy band models where delocalization is more important.

## 4.6 Nonradiative Transitions in Semiconductors

Finally nonradiative transitions which are specific for semiconductors are mentioned. In order to do so, we consider a specific radiative transition, viz. the donor-acceptor-pair emission (Sect. 3.3.9). In the excited state the donor and acceptor are occupied (Fig. 4.14). This excited luminescent center may show radiative and nonradiative transitions within the center itself (similar to the discussion in Sect. 4.2). In addition, however, there are other processes which are related to the valence and/or conduction band.

If the donor is thermally ionized (Fig. 4.14), the luminescence will be quenched unless it is trapped again at a donor site. A different nonradiative mechanism is

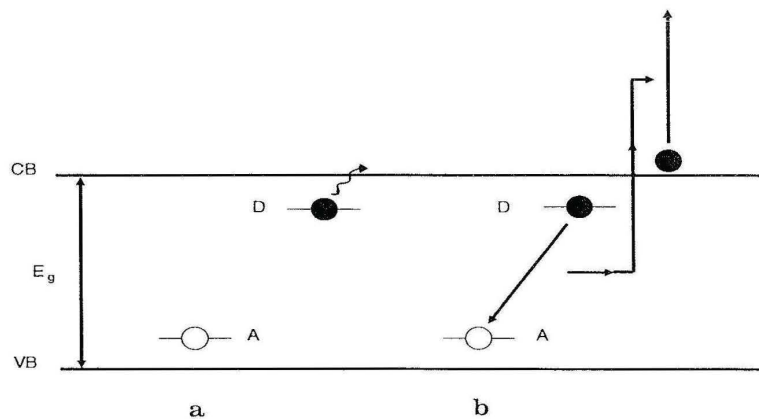


**Fig. 4.14.** Nonradiative transitions in a semiconductor. The donor-acceptor pair emission (DA) can be quenched by thermal ionization of one of the centers (*a*) or by an Auger process (*b*). In the latter case a conduction electron is promoted high into the conduction band

an Auger transition [17]. This is also illustrated in Figure 4.14. The energy of the excited donor-acceptor pair is used to excite a conduction band electron to a higher state in the conduction band. The hot conduction-band electron which has been created relaxes subsequently by intraband transitions. As a consequence the donor-acceptor pair emission is quenched.

More generally, an Auger transition can be defined as a transition in which energy is transferred from one electronic particle to another in such a way that in the final state the energy of one of the particles lies in a continuum. Auger processes can be classified as intrinsic or extrinsic. The former occur in the pure semiconductor, the latter involve electronic states of impurities like in the example in Figure 4.14. All types of luminescence transitions described in Section 3.3.9 can be quenched by Auger processes.

## References

1. DiBartolo B (ed) (1980) Radiationless processes. Plenum, New York
2. DiBartolo B (ed) (1991) Advances in nonradiative processes in solids. Plenum, New York
3. Struck CW, Fonger WH (1991) Understanding luminescence spectra and efficiency using  $W_p$  and related functions, Springer, Berlin Heidelberg New York
4. Yen WM, Selzer PM (eds) (1981) Laser spectroscopy of solids. Springer, Berlin Heidelberg New York
5. Riseberg LA, Weber MJ ((1976) Progress in optics. In: Wolf E (ed) vol XIV. North-Holland, Amsterdam
6. van Dijk JMF, Schuurmans MFH (1983), J Chem Phys 78:5317
7. Berdowski PAM, Blasse G (1984) Chem Phys Letters 107:351
8. de Hair JThW, Blasse G (1976) J Luminescence 14:307; J Solid State Chem 19:263
9. Blasse G, van Vliet JPM, Verweij JWM, Hoogendam R, Wiegel M (1989) J Phys Chem Solids 50:583
10. Sabbatini N, Blasse G (1988) J Luminescence 40/41:288

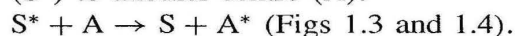
11. Bleijenberg KC, Blasse G (1979) *J Solid State Chem* 28:303
12. Bril A (1962) in Kallman and Spruch (eds), *Luminescence of organic and inorganic materials*. Wiley, New York p 479; de Poorter JA, Bril A (1975) *J Electrochem Soc* 122:1086
13. Robbins DJ (1980) *J Electrochem Soc* 127:2694
14. Moine B, Courtois B, Pedrini C (1989) *J Phys France* 50:2105
15. Blasse G, Schipper W, Hamelink JJ (1991) *Inorg Chim Acta* 189:77
16. Blasse G, p 314 in ref. 1
17. Williams F, Berry DE, Bernard JE, p 409 in ref. 1

## CHAPTER 5

# Energy Transfer

### 5.1 Introduction

In Chapter 2, the luminescent center was brought into the excited state, whereas in Chapters 3 and 4 the return to the ground state was considered, radiatively and nonradiatively, respectively. In this chapter another possibility to return to the ground state is considered, viz. by transfer of the excitation energy from the excited centre ( $S^*$ ) to another centre (A):



The energy transfer may be followed by emission from A. Species S is then said to sensitize species A. However,  $A^*$  may also decay nonradiatively; in this case species A is said to be a quencher of the S emission.

Energy transfer between two centres requires a certain interaction between these centres. Nowadays the process of energy transfer is a well-understood phenomenon of which the more important aspects will be discussed here. For more profound treatments the reader is referred to the literature cited [1-3].

The organization of this chapter is as follows. In Sect. 5.2, we consider energy transfer between a pair of unlike luminescent centers. The theories of Förster and Dexter will be introduced. In Sect. 5.3, the topic is extended to energy transfer between identical centers. As a consequence of this, the phenomenon of concentration quenching of luminescence takes place. The section is split into two parts, one dealing with centers to which the weak-coupling scheme applies, the other dealing with centers to which the strong-coupling scheme applies. In Sect. 5.4, energy transfer in semiconductors is very briefly mentioned.

### 5.2 Energy Transfer Between Unlike Luminescent Centers

Consider two centers, S and A, separated in a solid by distance R (Fig. 5.1). We use the (classic) notation S and A (for sensitizer and activator); other authors use D and A (for donor and acceptor). The energy level schemes are also given in Fig. 5.1. An asterisk indicates the excited state. Let us assume that the distance R is so short that the centres S and A have a non-vanishing interaction with each other. If S is in the excited state and A in the ground state, the relaxed excited state of S may transfer

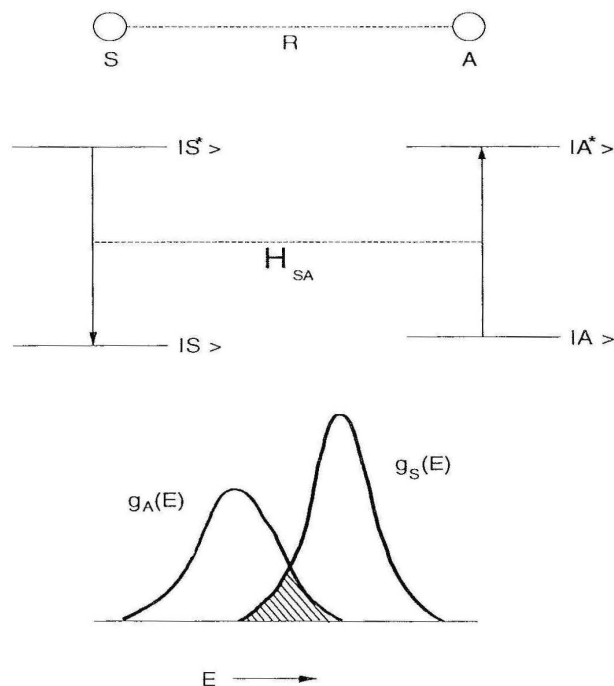


**Fig. 5.1.** Energy transfer between the centers S and A and an illustration of Eq. (5.1). The two centers are at a distance R (top). The energy level schemes and the interaction  $H_{SA}$  are given in the middle. The spectral overlap is illustrated at the bottom (hatched part)

its energy to A. The rate of such energy transfer processes has been calculated by Förster. Later Dexter extended this treatment to other interaction types.

Energy transfer can only occur if the energy differences between the ground- and excited states of S and A are equal (resonance condition) and if a suitable interaction between both systems exists. The interaction may be either an exchange interaction (if we have wave function overlap) or an electric or magnetic multipolar interaction. In practice the resonance condition can be tested by considering the spectral overlap of the S emission and the A absorption spectra. The Dexter result looks as follows:

$$P_{SA} = \frac{2\pi}{\hbar} | \langle S, A^* | H_{SA} | S^*, A \rangle |^2 \int g_S(E) \cdot g_A(E) dE \quad (5.1)$$

In Eq. (5.1) the integral presents the spectral overlap,  $g_X(E)$  being the normalized optical line shape function of centre X (see Fig. 5.1, where the spectral overlap has been hatched). Equation [5.1] shows that the transfer rate  $P_{SA}$  vanishes for vanishing spectral overlap. The matrix element in Eq. (5.1) represents the interaction ( $H_{SA}$  being the interaction Hamiltonian) between the initial state  $|S^*, A \rangle$  and the final state  $|S, A^* \rangle$ .

The distance dependence of the transfer rate depends on the type of interaction. For electric multipolar interaction the distance dependence is given by  $R^{-n}$  ( $n = 6, 8, \dots$

for electric-dipole electric-dipole interaction, electric-dipole electric-quadrupole interaction, ... respectively). For exchange interaction the distance dependence is exponential, since exchange interaction requires wave function overlap.

A high transfer rate, i.e. a high value of  $P_{SA}$ , requires a considerable amount of: (1) resonance, i.e. the S emission band should overlap spectrally the A absorption band(s), (2) interaction, which may be of the multipole-multipole type or of the exchange type. Only for some specific cases, is the interaction type known. The intensity of the optical transitions determines the strength of the electric multipolar interaction. High transfer rates can only be expected if the optical transitions involved are allowed electric-dipole transitions. If the absorption strength vanishes, the transfer rate for electric multipolar interaction vanishes too. However, the overall transfer rate does not necessarily vanish, because there may be contributions by exchange interaction. The transfer rate due to exchange interaction depends on wave function overlap (and, of course, spectral overlap), but not on the spectral properties of the transitions involved.

Over what distances can energy be transferred in this way? To answer this question it is important to realize that  $S^*$  has several ways to decay to the ground state: energy transfer with a rate  $P_{SA}$ , and radiative decay with a rate  $P_S$  (the radiative rate). We neglect nonradiative decay (but it can be included in  $P_S$ ). The critical distance for energy transfer ( $R_c$ ) is defined as the distance for which  $P_{SA}$  equals  $P_S$ , i.e. if S and A are separated by a distance  $R_c$ , the transfer rate equals the radiative rate. For  $R > R_c$  radiative emission from S prevails, for  $R < R_c$  energy transfer from S to A dominates.

If the optical transitions of S and A are allowed electric-dipole transitions with a considerable spectral overlap,  $R_c$  may be some 30 Å. If these transitions are forbidden, we need exchange interaction for the transfer to occur. This restricts the value of  $R_c$  to some 5–8 Å.

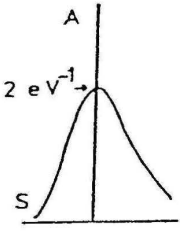
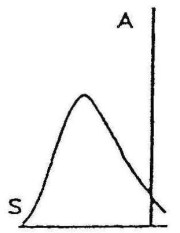
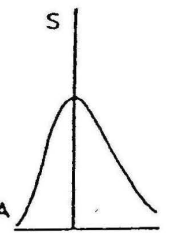
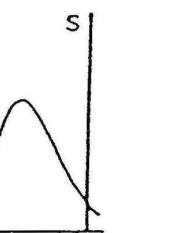
If the spectral overlap consists of a considerable amount of overlap of an emission band and an allowed absorption band, there can be a considerable amount of radiative energy transfer:  $S^*$  decays radiatively and the emitted radiation is reabsorbed. This can be observed from the fact that the emission band vanishes at the wavelengths where A absorbs strongly.

Energy transfer as described by Eq. (5.1) is nonradiative energy transfer. The occurrence of nonradiative energy transfer can be detected in several ways. If the excitation spectrum of the A emission is measured, the absorption bands of S will be found as well, since excitation of S yields emission from A via energy transfer. If S is excited selectively, the presence of A emission in the emission spectrum points to  $S \rightarrow A$  energy transfer. Finally, the decay time of the S emission should be shortened by the presence of nonradiative energy transfer, since the transfer process shortens the life time of the excited state  $S^*$ .

To obtain some feeling for transfer rates and critical distances, we will perform some simple calculations. We assume that the interaction is of the electric-dipolar type. In that case Eq. (5.1) together with  $P_{SA}(R_c) = P_S$  yields for  $R_c$  the following expression [4]:

$$R_c^6 = 3 \times 10^{12} \cdot f_A \cdot E^{-4} \cdot S_0 \quad (5.2)$$

**Table 5.1.** Schematic energy transfer calculations between a broad-band and a narrow-line centre (see text)

spectra*				
spectral overlap $\int g_S g_A^{dE}$	$2 \text{ eV}^{-1}$	$0.2 \text{ eV}^{-1}$	$2 \text{ eV}^{-1}$	$0.2 \text{ eV}^{-1}$
energy of maximum spectral overlap, E	3 eV	3 eV	3 eV	3 eV
oscillator strength accepting ion, $f_A$	$10^{-6}$	$10^{-6}$	$10^{-2}$	$10^{-2}$
$R_c$	6.5 Å	4.5 Å	30 Å	20 Å

\* S: sensitizer (energy-transferring ion).

A: activator (energy-accepting ion). Height at band maximum  $2 \text{ eV}^{-1}$ . Band width 0.5 eV.

Here  $f_A$  presents the oscillator strength [1,5] of the optical absorption transition on A, E the energy of maximum spectral overlap, and SO the spectral overlap integral as given in Eq. (5.1). Equation (5.2) makes it possible to calculate  $R_c$  from spectral data.

In Table 5.1 the results of the calculation are presented. An S and an A center are considered, and R is always 4 Å. Transfer from a broad-band emitter to a narrow-line absorber is considered (the first two cases) as well as the reverse. The spectral overlap is optimal (1<sup>st</sup> and 3<sup>rd</sup> case) or marginal. For the narrow-line absorber,  $f_A$  is taken to be  $10^{-6}$ , for the broad-band absorber  $10^{-2}$  (forbidden and allowed transitions, respectively). E is taken to be 3 eV. These values are rather realistic, although lower f values may occur.

From Table 5.1 we can learn the following:

- energy transfer from a broad-band emitter to a line absorber is only possible for nearest neighbours in the crystal lattice
- transfer from a line emitter to a band absorber proceeds over fairly long distances.

Let us finally illustrate Eq. (5.1) by some examples:

(a) The  $\text{Gd}^{3+}$  ion shows energy transfer from the  ${}^6\text{P}_{7/2}$  level to most rare earth ions, but not to  $\text{Pr}^{3+}$  and  $\text{Tm}^{3+}$ . Figure 2.14 shows that these two ions do not have energy



levels at the same energy as the  ${}^6P_{7/2}$  level, so that the resonance condition is not satisfied, the spectral overlap vanishes, and the transfer rate becomes zero.

(b) In  $\text{Ca}_5(\text{PO}_4)_3\text{F}:\text{Sb}^{3+},\text{Mn}^{2+}$  the  $\text{Sb}^{3+}$  ion can transfer energy to the  $\text{Mn}^{2+}$  ion. The  $\text{Sb}^{3+}$  emission covers several  $\text{Mn}^{2+}$  absorption transitions. These have very low  $f$  values (spin- and parity forbidden), and the transfer occurs by exchange interaction with  $R_c \sim 7 \text{ \AA}$ .

(c) In  $\text{Rb}_2\text{ZnBr}_4:\text{Eu}^{2+}$  two types of  $\text{Eu}^{2+}$  ions are found with different spectra due to the presence of two types of crystallographic sites for  $\text{Rb}^+$  in  $\text{Rb}_2\text{ZnBr}_4$ . Energy transfer occurs from the higher-emitting  $\text{Eu}^{2+}$  (415 nm) to the lower-emitting  $\text{Eu}^{2+}$  (435 nm). Since all optical transitions involved are allowed, it is not surprising that  $R_c$  has a high value (35  $\text{\AA}$ ) [6].

## 5.3 Energy Transfer Between Identical Luminescent Centers

If we consider now transfer between two identical ions, for example between S and S, the same considerations can be used. If transfer between two S ions occurs with a high rate, what will happen in a lattice of S ions, for example in a compound of S? There is no reason why the transfer should be restricted to one step, so that we expect that the first transfer step is followed by many others. This can bring the excitation energy far from the site where the absorption took place: energy migration. If in this way, the excitation energy reaches a site where it is lost nonradiatively (a killer or quenching site), the luminescence efficiency of that composition will be low. This phenomenon is called concentration quenching. This type of quenching will not occur at low concentrations, because then the average distance between the S ions is so large that the migration is hampered and the killers are not reached.

Energy migration in concentrated systems has been an issue of research over the last two decades. Especially since lasers became readily available, the progress has been impressive. Here we will first consider the case that S is an ion to which the weak-coupling scheme applies. In practice this case consists of the trivalent rare earth ions. Subsequently we will deal with the case where S is an ion to which the intermediate- or strong-coupling scheme applies.

### 5.3.1 Weak-Coupling Scheme Ions

At first sight, energy transfer between identical rare earth ions seems to be a process with a low rate, because their interaction will be weak in view of the well-shielded character of the  $4f$  electrons. However, although the radiative rates are small, the spectral overlap can be large. This originates from the fact that  $\Delta R \simeq 0$ , so that the absorption and emission lines will coincide. Further the transfer rate will easily surpass the radiative rate, since the latter is low. In fact energy migration has been

observed in many rare earth compounds, and concentration quenching usually becomes effective for concentrations of a few atomic percent of dopant ions. Energy transfer over distances of up to some  $10 \text{ \AA}$  is possible. As an example, we mention the transfer rate between  $\text{Eu}^{3+}$  ions or between  $\text{Gd}^{3+}$  ions which may be of the order of  $10^7 \text{ s}^{-1}$  if the distance is  $4 \text{ \AA}$  or shorter. This has to be compared with a radiative rate of  $10^2\text{--}10^3 \text{ s}^{-1}$ . Consequently the excitation energy may be transferred more than  $10^4$  times during the life time of the excited state.

This type of research uses pulsed and tunable lasers as an excitation source. The rare earth ion is excited selectively with a laser pulse, and its decay is analyzed. The shape of the decay curve is characteristic of the physical processes in the compound under study. For a detailed review the reader is referred to the literature [1–3]. Here we give some results for specific situations. We assume that the object of our study consists of a compound of a rare earth ion S which contains also some ions A which are able to trap the migrating excitation energy of S by SA transfer.

(1) If excitation into S is followed by emission from the same S ion (i.e. the isolated ion case), or if excitation into S is followed after some migration by emission from S only, the decay is described by

$$I = I_0 \exp(-\gamma t), \quad (5.3)$$

where  $I_0$  is the emission intensity at time  $t = 0$ , i.e. immediately after the pulse, and  $\gamma$  is the radiative rate. The decay is exponential. Equation (5.3) is identical to Eq. (3.3).

(2) If some SA transfer occurs, but no SS transfer at all, the S decay is given by

$$I = I_0 \exp(-\gamma t - Ct^{3/n}), \quad (5.4)$$

where C is a parameter containing the A concentration ( $C_A$ ) and the SA interaction strength, and  $n \geq 6$  depending on the nature of the multipolar interaction. This decay is not exponential. Immediately after the pulse the decay is faster than in the absence of A. This is due to the presence of SA transfer. After a long time the decay becomes exponential with the radiative rate as a slope. This represents the decay of S ions which do not have A ions in the surroundings.

(3) If we allow for SS transfer, the situation becomes difficult. We consider first the extreme case that the rate of SS transfer ( $P_{SS}$ ) is much higher than  $P_{SA}$  (fast diffusion). The decay rate is exponential and fast:

$$I = I_0 \exp(-\gamma t) \exp(-C_A \cdot P_{SA} \cdot t). \quad (5.5)$$

(4) If  $P_{SS} \ll P_{SA}$ , we are dealing with diffusion-limited energy migration. For  $t \rightarrow \infty$  the decay curve can be described by

$$I = I_0 \exp(-\gamma t) \exp(-11.404 C_A \cdot C^{1/4} \cdot D^{3/4} \cdot t) \quad (5.6)$$

if the sublattice of S ions is three dimensional. C is a parameter describing the SA interaction and D the diffusion constant of the migrating excitation energy. For lower dimensions non-exponential decays are to be expected.

In Fig. 5.2, we have given some of these decay curves. The temperature dependence of  $P_{SS}$  is very complicated. Due to inhomogeneous broadening, the S ions

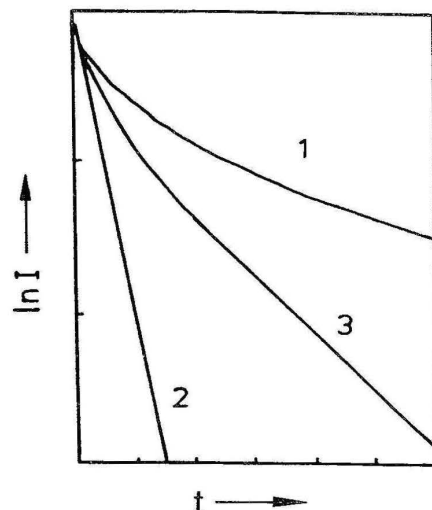


**Fig. 5.2.** Several possibilities for the decay curve of the excited S ion. The S emission intensity is plotted logarithmically versus time. Curve 1: no SS transfer (Eq. (5.3)); curve 2: rapid SS migration (Eq. (5.5)); curve 3: intermediate case (for example, Eq. (5.6))

are not exactly resonant, but their energy levels show very small mismatches. We need phonons to overcome these. At room temperature, the lines are broadened and phonons are available, so that these mismatches do not hamper the energy migration. However, at very low temperatures they hamper the energy migration, or make it even impossible. The theory of phonon-assisted energy transfer has been treated elsewhere [2]. For identical ions, one-phonon assisted processes are not of much importance. Two-phonon assisted processes have a much higher probability. One of these (a two-site nonresonant process) yields a  $T^3$  dependence. Another (a one-site resonant process), which uses a higher energy level gives an  $\exp(\frac{-\Delta E}{kT})$  dependence, where  $\Delta E$  is the energy difference between the level concerned and the higher level. Figure 5.3 gives a schematical presentation of these two processes.

Let us now consider some examples. First we consider  $\text{Eu}^{3+}$  compounds. In  $\text{EuAl}_3\text{B}_4\text{O}_{12}$ , there is a three-dimensional  $\text{Eu}^{3+}$  sublattice with shortest Eu–Eu distance equal to 5.9 Å. At 4.2 K there is no energy migration at all, but at 300 K diffusion-limited energy migration occurs. The temperature dependence of  $P_{SS}$  is exponential with  $\Delta E \sim 240 \text{ cm}^{-1}$ . This is due to the fact that the  $^5\text{D}_0$ – $^7\text{F}_0$  transition is forbidden under the relevant site symmetry ( $D_3$ ), so that the multipolar interactions vanish. The distance of 5.9 Å is prohibitive for transfer by exchange interaction. At higher temperatures the  $^7\text{F}_1$  level is thermally populated and multipolar interaction becomes effective. The experimental value of  $\Delta E$  corresponds to the energy difference  $^7\text{F}_0$ – $^7\text{F}_1$  (compare Fig. 2.14). Analysis shows that the excited state makes 1400 jumps during its life time at room temperature with a diffusion length of 230 Å. Table 5.2 gives values of the transfer rate and the diffusion constant, together with those for other  $\text{Eu}^{3+}$  compounds.

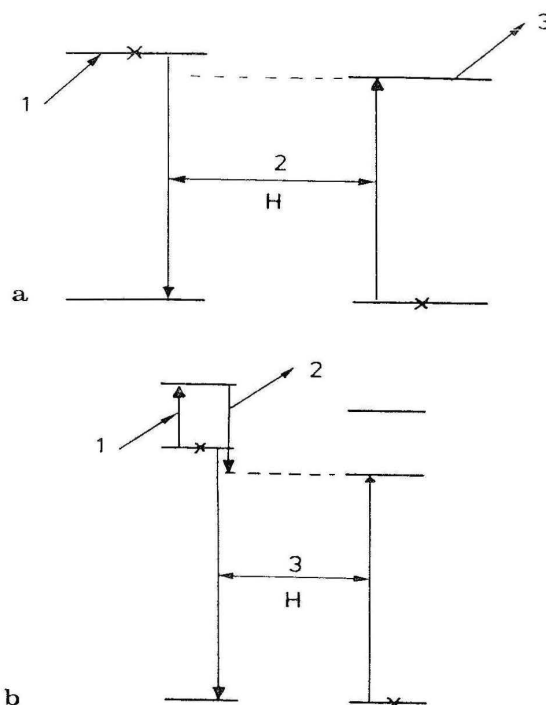


**Fig. 5.3.** A. Two-site nonresonant process in phonon-assisted energy transfer. (1) and (3) present the ion-phonon interaction, (2) the site-site coupling  $H$ . B. One-site resonant process in phonon-assisted energy transfer. (1) and (2) present the ion-phonon interaction, (3) the site-site coupling

**Table 5.2.** Energy migration characteristics in some  $\text{Eu}^{3+}$  compounds at 300 K (data from Ref. [7])

Compound	Shortest Eu–Eu distance	Diffusion constant ( $\text{cm}^2\text{s}^{-1}$ )	Hopping time <sup>d</sup> (s)
$\text{EuAl}_3\text{B}_4\text{O}_{12}$	5.9 Å	$8 \times 10^{-10}$	$8 \times 10^{-7}$
$\text{NaEuTiO}_4$	3.7 Å	$2 \times 10^{-8}$ <sup>a</sup>	$2 \times 10^{-8}$
$\text{EuMgB}_5\text{O}_{10}$	4.0 Å	$\sim 10^{-8}$	$\sim 10^{-7}$
$\text{Eu}_2\text{Ti}_2\text{O}_7$	3.7 Å	$9 \times 10^{-12}$ <sup>b</sup> $3 \times 10^{-9}$ <sup>c</sup>	$3 \times 10^{-5}$ <sup>b</sup> $8 \times 10^{-8}$ <sup>c</sup>
$\text{Li}_6\text{Eu}(\text{BO}_3)_3$	3.9 Å	$2 \times 10^{-9}$	$\sim 10^{-7}$
$\text{EuOCl}$	3.7 Å	$5.8 \times 10^{-10}$	$4 \times 10^{-7}$

<sup>a</sup>  $D = 8 \times 10^{-11} \text{ cm}^2\text{s}^{-1}$  at 1.2 K.

<sup>b</sup> values at 15 K.

<sup>c</sup> values at 43 K.

<sup>d</sup> average time for one  $\text{Eu}^{3+}$ - $\text{Eu}^{3+}$  transfer step.

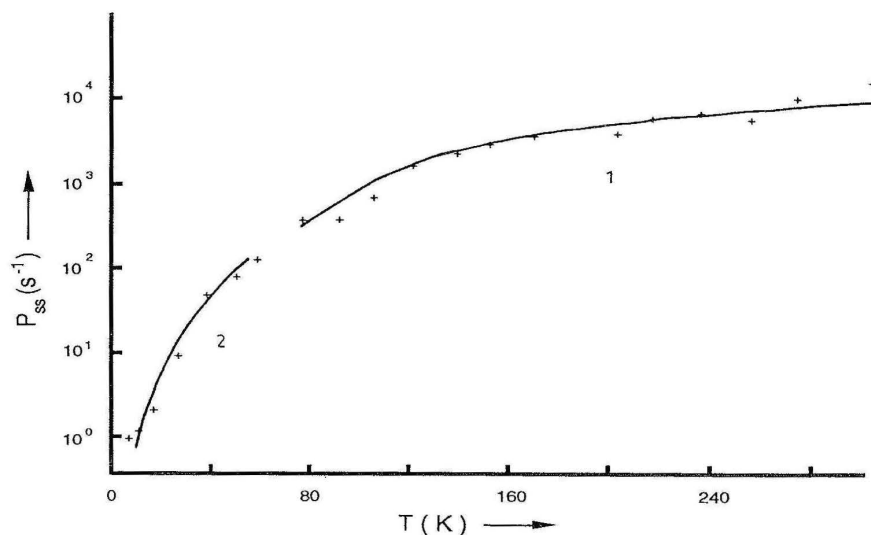


**Fig. 5.4.** Temperature dependence of the  $\text{Eu}^{3+}$ - $\text{Eu}^{3+}$  transfer rate in  $\text{EuMgB}_5\text{O}_{10}$ . Line 1 is a fit using thermally activated migration via the  ${}^7\text{F}_1$  level of the  $\text{Eu}^{3+}$  ion; line 2 is a fit to the  $T^3$  temperature dependence predicted by a two-site nonresonant process

Samples of  $\text{EuAl}_3\text{B}_4\text{O}_{12}$  which are so pure that the excited state does not reach a killer site during its life time, show efficient luminescence. Samples which contain a low concentration of killer sites do not show luminescence at 300 K. However, at 4.2 K they do, the migration being slowed down considerably or even completely. An example is a crystal of  $\text{EuAl}_3\text{B}_4\text{O}_{12}$ , grown from a  $\text{K}_2\text{SO}_4/\text{MoO}_3$  flux [8]. These crystals contain  $\sim 25$  ppm  $\text{Mo}^{3+}$  (on  $\text{Al}^{3+}$  sites). This ion is an efficient killer of the  $\text{Eu}^{3+}$  emission.

Two-dimensional energy migration was observed for  $\text{NaEuTiO}_4$  and  $\text{EuMgAl}_{11}\text{O}_{19}$ , and one-dimensional energy migration for  $\text{EuMgB}_5\text{O}_{10}$  and  $\text{Li}_6\text{Eu}(\text{BO}_3)_3$ . In the relevant crystal structures the  $\text{Eu}^{3+}$  ions form a two- and a one-dimensional sublattice, respectively.

The temperature dependence of  $P_{SS}$  is given for  $\text{EuMgB}_5\text{O}_{10}$  in Fig. 5.4. At lower temperatures, we find the  $T^3$  dependence expected for two-phonon assisted energy migration involving the  ${}^7\text{F}_0$  and  ${}^5\text{D}_0$  levels. At higher temperatures the temperature dependence becomes exponential, indicating transfer involving the  ${}^7\text{F}_1$  and  ${}^5\text{D}_0$  levels.

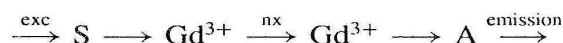
The situation in  $\text{Eu}^{3+}$  compounds can be characterized as follows:

- if the  $\text{Eu}$ - $\text{Eu}$  distance is larger than  $5 \text{ \AA}$ , exchange interaction becomes ineffective. Only multipolar interactions are of importance, and they will be weak anyhow. Actually, if sufficiently pure,  $\text{EuAl}_3\text{B}_4\text{O}_{12}$  ( $\text{Eu}$ - $\text{Eu}$   $5.9 \text{ \AA}$ ),  $\text{Eu}(\text{IO}_3)_3$  ( $\text{Eu}$ - $\text{Eu}$   $5.9 \text{ \AA}$ ), and  $\text{CsEuW}_2\text{O}_8$  ( $\text{Eu}$ - $\text{Eu}$   $5.2 \text{ \AA}$ ) luminesce efficiently at 300 K.
- if the  $\text{Eu}$ - $\text{Eu}$  distance is shorter than  $5 \text{ \AA}$ , exchange interaction becomes effective. Examples are the intrachain migration in  $\text{EuMgB}_5\text{O}_{10}$  and  $\text{Li}_6\text{Eu}(\text{BO}_3)_3$  and the

migration in  $\text{Eu}_2\text{O}_3$  which is more rapid than in other compounds, even at very low temperatures.

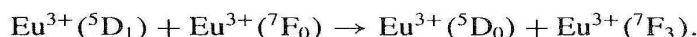
For  $\text{Tb}^{3+}$  compounds, the situation is not essentially different, but the temperature dependence of the transfer rate shows another behavior, because the  ${}^7\text{F}_6$  and  ${}^5\text{D}_4$  levels are connected by an optical transition with a higher absorption strength than the  ${}^7\text{F}_0$  and  ${}^5\text{D}_0$  levels in the case of  $\text{Eu}^{3+}$ .

Recently, there has been a lot of interest in energy migration in  $\text{Gd}^{3+}$  compounds, because this opens interesting possibilities for obtaining new, efficient luminescent materials (see Chapter 6). The  $\text{Gd}^{3+}$  sublattice is sensitized and activated. The sensitizer absorbs efficiently ultraviolet radiation and transfers this to the  $\text{Gd}^{3+}$  sublattice. By energy migration in this sublattice the activator is fed, and emission results. Absorption and quantum efficiencies of over 90% have been attained. The physical processes can be schematically presented as follows:



Here nx indicates the occurrence of many  $\text{Gd}^{3+}\text{--Gd}^{3+}$  jumps. A suitable choice of S is  $\text{Ce}^{3+}$ ,  $\text{Bi}^{3+}$ ,  $\text{Pr}^{3+}$  or  $\text{Pb}^{2+}$ . For A there are many possibilities:  $\text{Sm}^{3+}$ ,  $\text{Eu}^{3+}$ ,  $\text{Tb}^{3+}$ ,  $\text{Dy}^{3+}$ ,  $\text{Mn}^{2+}$ ,  $\text{UO}_6^{6-}$  and probably many more.

Not always is all of the excitation energy transferred. If only part of it is transferred, this is called cross-relaxation. Let us consider some examples. The higher-energy level emissions of  $\text{Tb}^{3+}$  and  $\text{Eu}^{3+}$  (Fig. 5.5) can also be quenched if the concentration is high. The following cross-relaxations may occur (compare Fig. 5.5):



The higher-energy level emission is quenched in favour of the lower energy level emission.

It is important to realize that we have met now two processes which will suppress higher-level emission, viz. multiphonon emission (Sect. 4.2.1) which is only of importance if the energy difference between the levels involved is less than about 5 times the highest vibrational frequency of the host lattice and which is independent of the concentration of the luminescent centres, and cross relaxation which will occur only above a certain concentration of luminescent centers since this process depends on the interaction between two centers.

Consider as an example the  $\text{Eu}^{3+}$  ion in  $\text{YBO}_3$  and  $\text{Y}_2\text{O}_3$ . For low  $\text{Eu}^{3+}$  concentrations (say 0.1 mole %) we find in  $\text{YBO}_3$  only  ${}^5\text{D}_0$  emission, since the higher-level emissions are quenched by multiphonon emission (highest borate frequency  $\sim 1050 \text{ cm}^{-1}$ ). In  $\text{Y}_2\text{O}_3$ , however, such a low concentration of  $\text{Eu}^{3+}$  ions gives  ${}^5\text{D}_3$ ,  ${}^5\text{D}_2$ ,  ${}^5\text{D}_1$  and  ${}^5\text{D}_0$  emission (highest lattice frequency  $\sim 600 \text{ cm}^{-1}$ ). For 3%  $\text{Eu}^{3+}$  in  $\text{Y}_2\text{O}_3$  the emission spectrum is dominated by the  ${}^5\text{D}_0$  emission. The higher-level emission is quenched by cross relaxation in favour of the  ${}^5\text{D}_0$  emission.

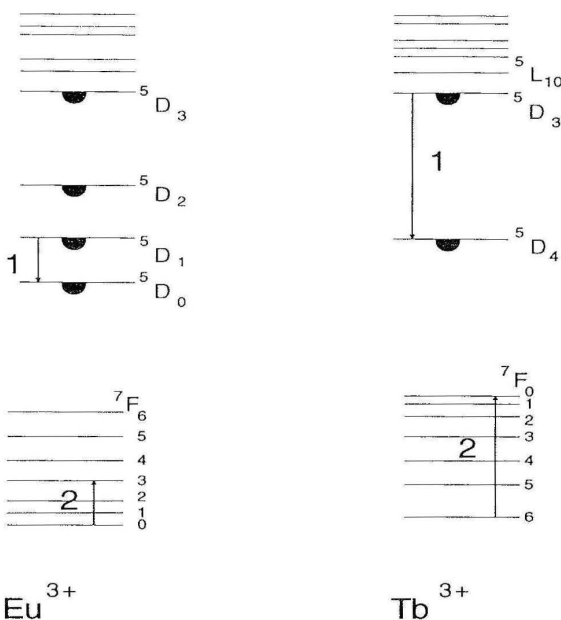


**Fig. 5.5.** Quenching of higher-level emission by cross relaxation. Left-hand side  $\text{Eu}^{3+}$ : the  ${}^5D_1$  emission on ion 1 is quenched by transferring the energy difference  ${}^5D_1 - {}^5D_0$  to ion 2 which is promoted to the  ${}^7F_3$  level. Right-hand side  $\text{Tb}^{3+}$ : the  ${}^5D_3$  emission on ion 1 is quenched by transferring the energy difference  ${}^5D_3 - {}^5D_4$  to ion 2 which is promoted to the  ${}^7F_0$  level

Up to now it has been demonstrated that concentration quenching of the luminescence of rare earth compounds consists of energy migration to killers in the case of  $\text{Eu}^{3+}$ ,  $\text{Gd}^{3+}$ ,  $\text{Tb}^{3+}$ . In the case of  $\text{Sm}^{3+}$  and  $\text{Dy}^{3+}$ , the above-mentioned cross relaxation is responsible for concentration quenching: the quenching of the luminescence occurs in ion pairs and not by migration. For other rare earth ions the situation is in between. We can use  $\text{Pr}^{3+}$  to illustrate the situation, and consider, in addition to energy migration, cross relaxation between  $\text{Pr}^{3+}$  ions, i.e. every  $\text{Pr}^{3+}$  ion can be a killer of its neighbours luminescence. Figure 5.6 gives possible cross relaxation processes which quench the  ${}^3P_0$  and the  ${}^1D_2$  emission of  $\text{Pr}^{3+}$ . The situation is even more complicated, because quenching may also occur in the isolated  $\text{Pr}^{3+}$  ion due to multiphonon emission if the available frequencies are high enough. The energy gap below the  ${}^3P_0$  level is  $3500 \text{ cm}^{-1}$ , that below the  ${}^1D_2$  level  $6500 \text{ cm}^{-1}$  (see Fig. 5.6). Since the probability of all these processes depends strongly on the nature of the lattice and its constituents, the luminescence behaviour of  $\text{Pr}^{3+}$  compounds is expected to vary strongly from case to case. This is what has been observed.

Extensive research has been performed on the system  $(\text{La,Pr})\text{F}_3$ . The  ${}^3P_0 - {}^1D_2$  nonradiative rate is very slow. At very low temperatures there is no energy migration due to small energy mismatches. Quenching of the  ${}^3P_0$  emission occurs only by cross relaxation. At higher temperatures, however, energy migration among the  ${}^3P_0$  level takes over. The Pr-Pr interaction is of the exchange type. The situation is different in

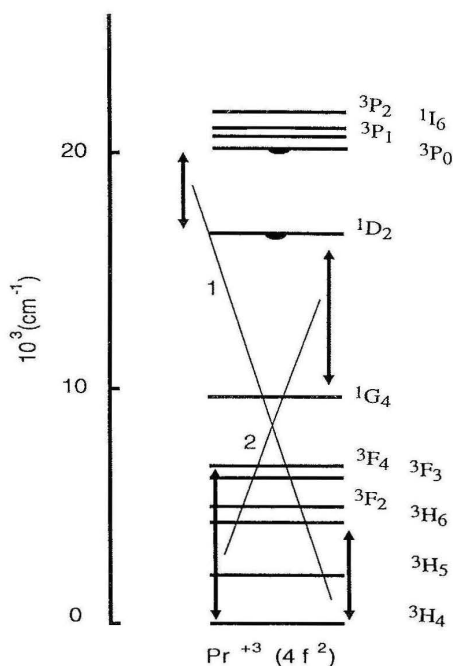


**Fig. 5.6.** The  $^3P_0$  and the  $^1D_2$  emission of  $\text{Pr}^{3+}$  can be quenched by cross relaxation as indicated by processes 1 and 2, respectively

a compound like  $\text{PrP}_5\text{O}_{14}$ . The high-energy vibrations of the phosphate group make the nonradiative  $^3P_0 \rightarrow ^1D_2$  transition the more probable process.

An interesting aspect of energy migration in concentrated rare-earth compounds is the influence of the magnetic order on the migration process. This has been studied on compounds of  $\text{Gd}^{3+}$  and  $\text{Tb}^{3+}$  by Jacquier et al. [9]. As an example we mention  $\text{GdAlO}_3$  and  $\text{TbAlO}_3$  which become antiferromagnetic at 3.9 K and 3.8 K, respectively. In the paramagnetic phase the experimental decays are in agreement with fast diffusion energy transfer. Below the Néel temperature, however, the decays are no longer exponential and considerably slower. The migration has become diffusion limited. The diffusion constants reported are  $1.6 \times 10^{-9} \text{ cm}^2\text{s}^{-1}$  at 4.4 K for both compounds, but only  $8 \times 10^{-12} \text{ cm}^2\text{s}^{-1}$  and  $8 \times 10^{-14} \text{ cm}^2\text{s}^{-1}$  at 1.6 K for  $\text{GdAlO}_3$  and  $\text{TbAlO}_3$ , respectively. In the antiferromagnetic phase the migration of excitation energy is slowed down, because nearest neighbour  $\text{Gd}^{3+}$  (or  $\text{Tb}^{3+}$ ) ions are oriented antiparallel, which makes energy transfer by exchange interaction impossible. In  $\text{EuAlO}_3$  such an effect does not occur. The  $\text{Eu}^{3+}$  ions (ground state  $^7F_0$ ) do not carry a magnetic moment. This compound is another example of a  $\text{Eu}^{3+}$  compound in which energy migration occurs down to the lowest temperatures due to exchange interaction.

Let us now turn to energy migration in concentrated systems for which the weak-coupling scheme is no longer valid.



### 5.3.2 Intermediate- and Strong-Coupling Scheme Ions

Whether or not energy transfer will occur between identical ions with  $S > 1$ , depends in the first place on the spectral overlap of their emission and absorption spectra. The reader will feel intuitively that for ions with strongly Stokes-shifted emission ( $S > 10$ ) this spectral overlap will be very small or even vanish, so that energy transfer becomes impossible.

It is easy to make these feelings more quantitative [10]. Consider a system of two identical luminescent centers. The ground state of each center is denoted by  $|g(i)v(i)\rangle$ , and the excited state by  $|e(i)v'(i)\rangle$ . Here  $g$  and  $e$  indicate the electronic states (ground or excited state) and  $v$  and  $v'$  the vibrational states, and  $i$  numbers the centers, i.e. 1 or 2.

If  $H$  presents the interaction causing energy transfer, the transition matrix element is given by

$$M = \langle g(1)v(1), e(2)v'(2) | H | e(1)v'(1), g(2)v(2) \rangle \quad (5.7)$$

If  $H$  operates on the electronic functions only,

$$M = \langle g(1)e(2) | H | e(1)g(2) \rangle \langle v(1) | v'(1) \rangle \langle v'(2) | v(2) \rangle. \quad (5.8)$$

The transfer probability is proportional to  $M^2$ , i.e. to  $|\langle v(1) | v'(1) \rangle|^4$ . At low temperatures the transfer transitions are restricted to the zero-vibrational levels, so that at 0K

$$M^2 \sim |\langle 0 | 0 \rangle|^4. \quad (5.9)$$

Here  $|0\rangle$  denotes the zero-vibrational level. At low temperatures, therefore, the transfer probability vanishes if the spectra do not show vibrational structure with a zero-phonon line.

A clear example is  $\text{CaWO}_4$ . The excitation energy on the tungstate group remains localized at that center in spite of nearby tungstate groups. However,  $\langle 0 | 0 \rangle$  is practically zero, so that  $P_{SS}$  vanishes.

At higher temperatures the occupation of vibrational levels is no longer restricted to the zero-vibrational levels. The spectral bands broaden, and, as a consequence the spectral overlap may increase enough to make (thermally stimulated) energy transfer possible. We will now discuss several examples for illustration [7,10].

The first case to be considered here is the luminescence of complexes with  $\text{U}^{6+}$  as the central ion. Their spectra consist of zero-vibrational transitions followed by a rich vibrational structure (see Fig. 3.5). Examples are  $\text{UO}_2^{2+}$ , octahedral  $\text{UO}_6^{6-}$ , trigonal prismatic  $\text{UO}_6^{6-}$  and tetrahedral  $\text{UO}_4^{2-}$ .

The presence of a zero-phonon line implies that the spectral overlap does not vanish, so that transfer between two identical species may occur if the interaction is strong enough. This has actually been observed. Several uranates have been studied and it was shown that the absorbed excitation energy migrates over the uranium lattice. At low temperatures this energy is usually captured by optical traps, i.e. species with a slightly different crystal field, and therefore different energy level diagram.

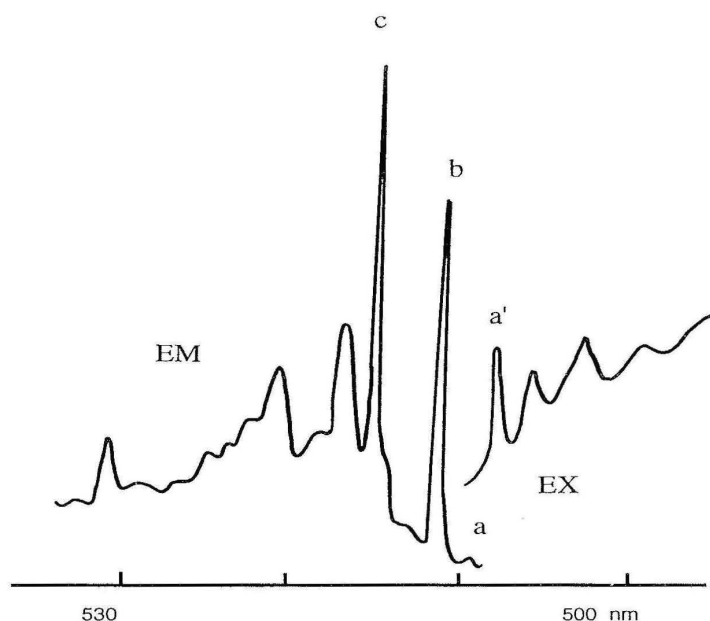


**Fig. 5.7.** Part of the emission and excitation spectrum of  $\text{Ba}_2\text{CaUO}_6$  at 4.2 K. The zero-phonon line in the excitation spectrum is indicated by  $a'$ . There is no corresponding line in the emission spectrum. The lines  $a$ ,  $b$  and  $c$  in the emission spectrum are the zero-phonon lines of the emission spectra belonging to three different uranate centres. This shows that excitation of the intrinsic uranate centres (with line  $a'$ ) is followed by energy migration to the extrinsic or defect uranate centres (with lines  $a$ ,  $b$  and  $c$ )

The emission originates from these traps, so that the zero-phonon line in emission is at slightly lower energy than that in absorption (see Fig. 5.7). The energy difference between these two zero-phonon lines is equal to the depth of these traps. At higher temperatures the traps are no longer effective, because they are too shallow. In uranates the luminescence is then usually quenched due to energy migration to  $\text{U}^{5+}$  centers. The latter act as quenching centers. In uranyl compounds, which are closer to stoichiometry, often strong intrinsic uranyl emission is observed, the quenching center concentration being too low to capture a substantial part of the excitation energy. Examples are  $\text{Cs}_2\text{UO}_2\text{Cl}_4$  and  $\text{UO}_2(\text{NO}_3)_2 \cdot 6\text{H}_2\text{O}$ .

Another intermediate coupling case is the  $\text{Bi}^{3+}$  ion in  $\text{Cs}_2\text{Na}(\text{Y},\text{Bi})\text{Cl}_6$ . The spectra show zero-vibrational transitions accompanied by many vibronic transitions. Energy migration among the  $\text{Bi}^{3+}$  ions occurs even at low  $\text{Bi}^{3+}$  concentrations. For  $\text{Cs}_2\text{NaBiCl}_6$  the intrinsic  $\text{Bi}^{3+}$  emission is no longer observed. Only a red broad-band emission appears. This has been ascribed to a  $\text{Bi}^{3+}$  ion next to impurity ions (like oxygen). This center is fed by energy migration over the  $\text{Bi}^{3+}$  ions followed by transfer to the impurity centers (trapping).

However, as we have seen above, a completely different situation may appear in other  $\text{Bi}^{3+}$  compounds (see also Sect. 3.3.7). In  $\text{Bi}_4\text{Ge}_3\text{O}_{12}$ , for example, excitation into a  $\text{Bi}^{3+}$  ion is followed by a pronounced relaxation, resulting in an emission with

a large Stokes shift (strong-coupling scheme). As a consequence, the relaxed excited state is out of resonance with the neighbouring ions, so that the excitation energy remains on the excited  $\text{Bi}^{3+}$  ion and energy migration does not occur.

The  $\text{Ce}^{3+}$  ion is another case where the Huang-Rhys parameter may vary considerably, so that the Stokes shift varies, and energy migration may or may not occur. The optical transitions are of the  $f-d$  type and as such allowed. In  $\text{CeBO}_3$  the  $\text{Ce}^{3+}$  emission at 300 K is quenched by energy migration to killer sites. The spectral overlap between absorption and emission is large. In  $\text{CeF}_3$ , however, the spectral overlap is much smaller. As a consequence no  $\text{Ce}^{3+}-\text{Ce}^{3+}$  energy transfer occurs: the emission of  $\text{CeF}_3$  is not quenched at room temperature due to a stronger relaxation. In fact  $\text{CeF}_3$  is proposed for important scintillator applications (see Chapter 9). The same situation occurs for  $\text{CeMgAl}_{11}\text{O}_{19}$ , an important host lattice for a green lamp phosphor, viz.  $\text{CeMgAl}_{11}\text{O}_{19}-\text{Tb}$ . If a  $\text{Ce}^{3+}$  compound does not show energy migration among the  $\text{Ce}^{3+}$  sublattice (like  $\text{CeF}_3$  or  $\text{CeMgAl}_{11}\text{O}_{19}$ ), large quantities of  $\text{Tb}^{3+}$  are necessary to quench the  $\text{Ce}^{3+}$  emission by  $\text{Ce}^{3+}-\text{Tb}^{3+}$  transfer. This is quite understandable, since the range of the  $\text{Ce}^{3+}-\text{Tb}^{3+}$  transfer is restricted.

Another case of strong coupling is formed by groups like tungstate and vanadate (see Sects. 2.3.2 and 3.3.5). These are oxidic anions with a central metal ion which has lost all its  $d$  electrons. Examples are  $\text{WO}_4^{2-}$ ,  $\text{WO}_6^{6-}$ ,  $\text{VO}_4^{3-}$ ,  $\text{MoO}_4^{2-}$ . Usually the Stokes shift of their emission is so large ( $\sim 16\,000\text{ cm}^{-1}$ ), that energy migration is completely hampered, even at room temperature. A well known example is  $\text{CaWO}_4$ . However, in other cases thermally-activated energy migration occurs, e.g. in  $\text{YVO}_4$ ,  $\text{Ba}_2\text{MgWO}_6$  and  $\text{Ba}_3\text{NaTaO}_6$ . In these compounds the Stokes shift is considerably smaller ( $\sim 10\,000\text{ cm}^{-1}$ ). This makes  $\text{YVO}_4-\text{Eu}^{3+}$  a very efficient red phosphor: excitation into the vanadate group is followed by energy migration over the vanadate groups to  $\text{Eu}^{3+}$  centers. Pure  $\text{YVO}_4$  emits only weakly at room temperature. However, if the temperature is lowered, or the  $\text{V}^{5+}$  concentration lowered by  $\text{P}^{5+}$  substitution, the migration is hampered,  $\text{YVO}_4$  starts to emit efficiently, and  $\text{YVO}_4-\text{Eu}^{3+}$  yields blue vanadate emission upon vanadate excitation.

This “dilution experiment”, in which  $\text{V}^{5+}$  is replaced by  $\text{P}^{5+}$ , has no consequences in the case of  $\text{CaWO}_4$  and  $\text{YNbO}_4$ , for example. The composition  $\text{CaSO}_4:W$  shows exactly the same luminescence as  $\text{CaWO}_4$ , and  $\text{YTbO}_4:\text{Nb}$  the same as  $\text{YNbO}_4$ . This proves that the luminescent  $\text{WO}_4^{2-}$  and  $\text{NbO}_4^{3-}$  groups in  $\text{CaWO}_4$  and  $\text{YNbO}_4$ , respectively, are to be considered as isolated luminescent centers in spite of the short distance to their nearest neighbours. This is due to the larger relaxation in the excited state in the cases of niobate and tungstate relative to vanadate, as is immediately clear from the larger Stokes shift ( $16\,000$  vs  $10\,000\text{ cm}^{-1}$ ). The fundamental reason for this fact is, however, not yet clear.

Up till here, it has been assumed in this chapter that free charge carriers do not play a role. This is different in the case of semiconductors.

## 5.4 Energy Transfer in Semiconductors

If excitation of a luminescent material results in the creation of free charge carriers, additional forms of energy transfer will take place. It is here not the place to consider these in detail (see, for example, Refs [11-13]).

Energy absorbed by the formation of free charge carriers can be transported through the crystal lattice. It should be realized that electrons and holes must move into the same direction (ambipolar diffusion). Therefore, the energy transport is determined by the carriers which have the shorter lifetime and the smaller diffusion constant. As discussed above (Sect. 3.3.9), the charge carriers will be trapped at centers in the crystal lattice where radiative recombination is one of the possibilities of returning to the ground state.

Energy transfer can also occur by excitons. An exciton is an excited state of the crystal lattice in which an electron and a hole are bound and can propagate through the lattice [14]. They can be divided into two classes, viz. Frenkel and Wannier excitons. In the former the electron-hole separation is of the order of an atomic radius, i.e. it can be considered as a localized excitation. In the latter this separation is large in comparison with the lattice constant. Consequently, its binding energy is much smaller than that of the Frenkel exciton.

Examples of Frenkel excitons were met above ( $\text{YVO}_4$ ,  $\text{CaWO}_4$ ,  $\text{Bi}_4\text{Ge}_3\text{O}_{12}$ ). An extreme case is solid Kr with an exciton binding energy of  $\sim 2$  eV and a radius of  $\sim 2$  Å. Semiconductors are examples in which Wannier excitons occur (e.g. Ge, GaAs, CdS, TlBr). As an extreme example we mention InSb with an exciton binding energy of  $\sim 0.6$  meV and a radius of  $\sim 600$  Å. Such an exciton is only stable at very low temperatures [15].

Free excitons can be bound to defects or become self trapped. In both cases the electron and hole will recombine, either radiatively or nonradiatively. An example was discussed in Sect. 3.3.1. It will be clear that energy transfer by excitons is of a general importance and occurs in semiconductors as well as in insulators.

The contents of Chapters 2–5 form the fundamental background knowledge which is necessary for a discussion of luminescent materials (Chapters 6–10). The reader should realize, however, that the treatment has been kept as simple and restricted as possible.

## References

1. Henderson B, Imbusch GF (1989) Optical spectroscopy of inorganic solids. Clarendon, Oxford
2. Yen WM, Selzer PM (eds) (1981) Laser spectroscopy of solids, Topics in Applied Physics 49. Springer, Berlin Heidelberg New York
3. Di Bartolo B (ed) (1984) Energy transfer processes in condensed matter. Plenum, New York
4. Blasse G (1987) Mat Chem Phys 16 (1987) 201; (1969) Philips Res Repts 24:131
5. Atkins PW (1990) Physical chemistry, 4th edn, Oxford University Press, Oxford
6. Blasse G (1986) J Solid State Chem 62:207

7. Blasse G (1988) *Progress Solid State Chem* 18:79
8. Kellendonk F, Blasse G (1981) *J Chem Phys* 75:561
9. Salem Y, Joubert MF, Linarrs C, Jacquier B (1988) *J Luminescence* 40/41:694
10. Powell RC, Blasse G (1980) *Structure and Bonding* 42:43
11. Bernard JE, Berry DE, Williams F, p 1 in Ref. [3]
12. Klingshirn C, p 285 in Ref. [3]
13. Broser I (1967) In: Aven M, Prener JS (eds) *Physics and chemistry of II-VI compounds*. North Holland, Amsterdam, Chapter 10
14. See e.g. C. Kittel, *Introduction to solid state physics*, Wiley, New York, several editions
15. Sturge MD (1982) In: Rashba ÉI, Sturge MD (eds) *Excitons*. North Holland, Amsterdam, Chapter 1

## CHAPTER 6

# Lamp Phosphors

### 6.1 Introduction

The previous chapters presented an outline of the phenomenon of luminescence in solids. They form the background for the following chapters which discuss luminescent materials for several applications, viz. lighting (Chapter 6), television (Chapter 7), X-ray phosphors and scintillators (Chapters 8 and 9), and other less-general applications (Chapter 10). These chapters will be subdivided as follows:

- the principles of the application
- the preparation of the materials
- the luminescent materials which were or are in use or have a strong potential to become used; a discussion of their luminescence properties in terms of Chapters 2–5
- problems in the field.

The emphasis will be on the materials in view of the topic of this book.

### 6.2 Luminescent Lighting [1-3]

Luminescent lighting started even before the Second World War\*. The ultraviolet radiation from a low-pressure mercury discharge is converted into white light by a phosphor layer on the inner side of the lamp tube. These lamps are much more efficient than the incandescent lamp: a 60 W incandescent lamp yields 15 lm/W, a standard 40 W luminescent lamp 80 lm/W.

A luminescent lamp is filled with a noble gas at a pressure of 400 Pa, containing 0.8 Pa mercury. In the discharge the mercury atoms are excited. When they return to the ground state, they emit (mainly) ultraviolet radiation. About 85% of the emitted radiation is at 254 nm and 12% at 185 nm. The remaining 3% is found in the longer wavelength ultraviolet and visible region (365, 405, 436 and 546 nm).

---

\* We use the term luminescent lighting instead of the generally used fluorescent lighting, since most of the luminescent materials that are used do not show fluorescence (which is defined as an emission transition without spin reversal, i.e.  $\Delta S = 0$ ; see also Appendix III).

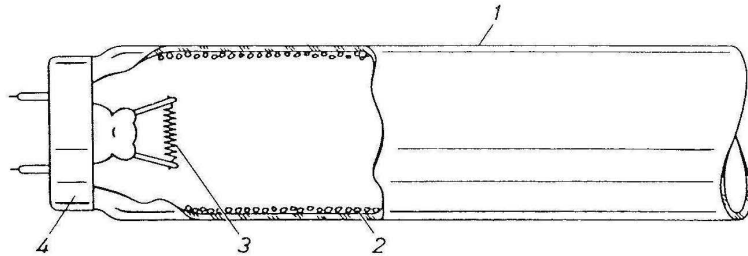


**Fig. 6.1.** Cross section of a low-pressure luminescent lamp. 1 glass tube; 2 luminescent powder; 3 cathode; 4 lamp cap

The lamp phosphor converts the 254 and 185 nm radiation into visible light (Fig. 6.1). It is in direct contact with the mercury discharge which rules out many potential candidates. For example, sulfides cannot be used in lamps since they react with mercury. A lamp phosphor should absorb the 254 and 185 nm radiation strongly and convert the absorbed radiation efficiently, i.e. their quantum efficiency should be high.

A luminescent lighting lamp has to emit white light, so that the sun, our natural lighting source, is imitated. The sun is a black body radiator, so that its emission spectrum obeys Planck's equation:

$$E(\lambda) = \frac{A\lambda^{-5}}{\exp(B/T_c) - 1} \quad (6.1)$$

Here A and B are constants,  $\lambda$  the emission wavelength and  $T_c$  the temperature of the black body. With increasing  $T_c$  the color of the radiator moves from (infra)red into the visible. In luminescent lamp terminology, "white" is used for 3500 K light, "cool-white" for 4500 K, and "warm-white" for 3000 K.

According to the principles of colorimetry, each color can be matched by mixing three primary colors. It is possible to represent colors in a color triangle [2]. Most currently used is the chromaticity diagram standardized by the Commission Internationale d'Eclairage. It is depicted in Fig. 6.2. For a definition of the color coordinates x and y, see Refs. [2] and [3]. The real colors cover an area enclosed by the line representing the spectral colors and the line connecting the extreme violet and the extreme red. The points within this area represent unsaturated colors.

The color points corresponding to Eq. (6.1) are given by the black body locus (BBL). Colors lying on the BBL are considered to be white. White light can be generated in different ways. The simplest one is to mix blue and orange. However, it is also possible to mix blue, green and red. Blending a number of emission bands into a continuous spectrum also yields, of course, white light. All these examples of color mixing are used in lamps, as we will see below.

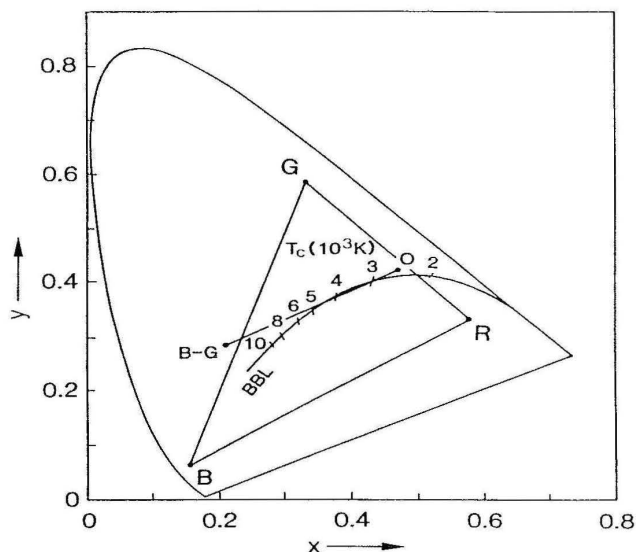


**Fig. 6.2.** CIE chromaticity diagram with black body locus (BBL). See also text. Reproduced with permission from Ref. [3]

Apart from the color point, there is another important lamp characteristic, viz. the color rendition. This property depends on the spectral energy distribution of the emitted light. It is characterized by comparing the color points of a set of test colors under illumination with the lamp to be tested and with a black body radiator. The color rendering index (CRI) equals 100 if the color points are the same under illumination with both sources. Under illumination with a lamp with low CRI, an object does not appear natural to the human eye.

In addition to the low-pressure mercury lamp discussed above, there is the high-pressure mercury lamp (Fig. 6.3). The gas discharge is contained in a small envelope surrounded by a larger bulb. The phosphor coating is applied to the inside of the outer bulb, so that there is no contact with the discharge.

In the high-pressure lamp the discharge also shows strong lines at 365 nm. The ideal phosphor for this lamp should, therefore, not only absorb short-wavelength ultraviolet radiation, but also long-wavelength. Further this discharge shows a considerable amount of blue and green emission. However, it is deficient in red. The phosphor has to compensate for this deficiency, so that it should have a red emission.

The phosphor temperature in the high-pressure lamp increases to 300°C, so that the emission should have a very high quenching temperature.

Since high-pressure lamps are used for outdoor lighting, the requirements for color rendition are less severe than for low-pressure lamps. However, if the phosphor is left out, red objects appear to be dull brown: this not only makes human skin look terrible, but also finding a red car in a parking lot problematic.



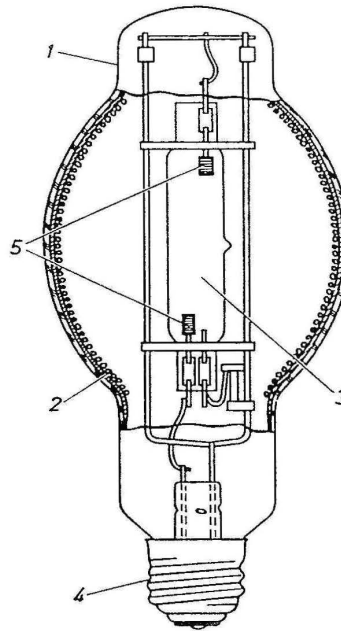


**Fig. 6.3.** Cross section of a high-pressure luminescent lamp. 1 glass bulb; 2 luminescent powder; 3 quartz envelope for gas discharge; 4 lamp cap; 5 electrodes

### 6.3 The Preparation of Lamp Phosphors

The lamp bulbs are coated with phosphor by using a suspension of phosphor powder particles. A lamp phosphor is therefore prepared as a powder. In principle this is done by standard solid state techniques in which intimate mixtures of starting materials are fired under a controlled atmosphere [4]. As a simple example we consider  $\text{MgWO}_4$ : it is prepared by mixing basic magnesium carbonate and tungsten trioxide in open silica crucibles at about  $1000^\circ\text{C}$ . Much more complicated is the case of the calcium halophosphate phosphor  $\text{Ca}_5(\text{PO}_4)_3(\text{F},\text{Cl})$ : Sb, Mn which is made by firing a mixture of  $\text{CaCO}_3$ ,  $\text{CaHPO}_4$ ,  $\text{CaF}_2$ ,  $\text{NH}_4\text{Cl}$ ,  $\text{Sb}_2\text{O}_3$  and  $\text{MnCO}_3$ . Actually the history of the preparation of this material is a beautiful illustration that increasing control and knowledge yields results: the light output of this phosphor has increased considerably during a long period of time. For more details the reader is referred to Chapter 3 in Ref. [2].

The luminescent activator concentration is of the order of 1%. Therefore high-quality starting materials and a clean production process are prerequisite for obtaining luminescent materials with a high efficiency. The controlled atmosphere is necessary to master the valence of the activator (for example  $\text{Eu}^{2+}$  or  $\text{Eu}^{3+}$ ) and the stoichiometry of the host lattice. Also the particle-size distribution of the phosphor needs to be controlled; this depends on the specific material under consideration.

In order to obtain homogeneous phosphors it is often necessary to leave the simple solid state technique. Coprecipitation may be of importance, especially if the activator and the host lattice ions are chemically similar. This is, of course, the case with rare-earth activated phosphors. For example,  $\text{Y}_2\text{O}_3:\text{Eu}^{3+}$  can be prepared profitably by coprecipitating the mixed oxalates from solution and firing the precipitate [5]. Actually the mixed oxides have become available commercially.

Usually phosphors decline slowly during lamp life [2]. This can be due to several processes:

- photochemical decomposition by 185 nm radiation from the mercury discharge (an illustrative approach to this problem is given in Ref. [6])
- reaction with excited mercury atoms from the discharge
- diffusion of sodium ions from the glass.

Quite often, coarse phosphors appear to be more stable than fine-grained phosphors. Obviously a high specific surface makes the phosphors more sensitive to interaction with radiation, mercury, and so on. This does not come as a surprise.

## 6.4 Photoluminescent Materials

### 6.4.1. Lamp Phosphors for Lighting

#### 6.4.1.1. Early Phosphors

In the early period of luminescent lighting (1938–1948), a mixture of two phosphors was used, viz.  $\text{MgWO}_4$  and  $(\text{Zn,Be})_2\text{SiO}_4:\text{Mn}^{2+}$ . The tungstate has a broad bluish-white emission band with a maximum near 480 nm (Fig. 6.4) and can be efficiently excited with short wavelength ultraviolet radiation. The emission spectrum of  $(\text{Zn,Be})_2\text{SiO}_4:\text{Mn}^{2+}$  is given in Fig. 6.5. It covers the green to red part of the visible spectrum.

The phosphor  $\text{MgWO}_4$  is an example of a luminescent material with 100% activator concentration, since each octahedral tungstate group in the lattice is able to luminesce. However, there is no concentration quenching. This is due to the large

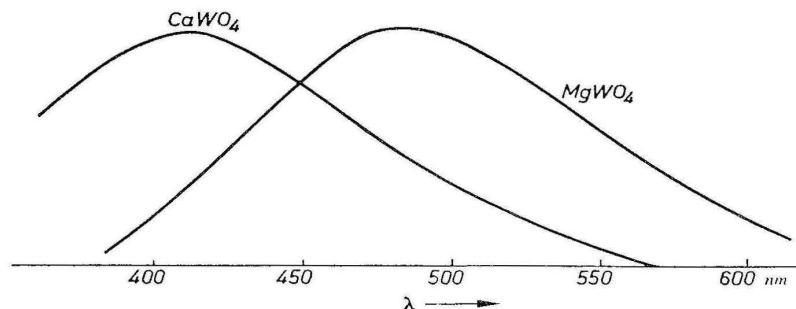
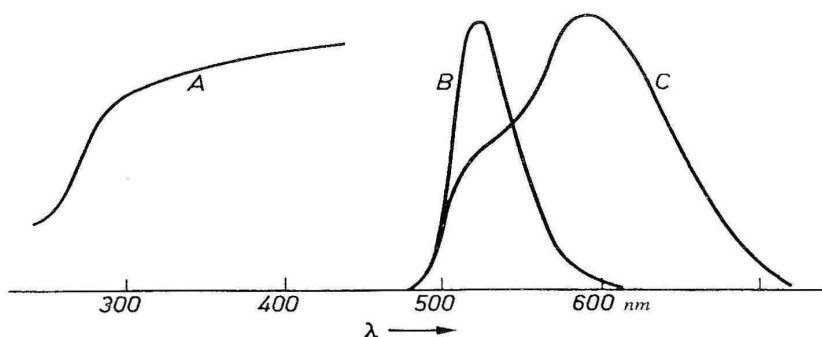


Fig. 6.4. Emission spectra of  $\text{MgWO}_4$  and  $\text{CaWO}_4$



**Fig. 6.5.** Emission spectra of  $\text{Zn}_2\text{SiO}_4:\text{Mn}^{2+}$  (B) and  $(\text{Zn,Be})_2\text{SiO}_4:\text{Mn}^{2+}$  (C). Curve A gives the diffuse reflection spectrum of  $\text{Zn}_2\text{SiO}_4:\text{Mn}^{2+}$

Stokes shift of the emission which brings the relaxed emitting state out of resonance with the neighbors. This, in turn, can be related to the nature of the optical transition which is a charge-transfer transition in the tungstate group. Therefore  $\Delta R$  in Fig. 2.3 is large. This yields not only a strongly Stokes-shifted emission, but also a very broad emission which is of importance for the color rendering.

The broadness of the  $(\text{Zn,Be})_2\text{SiO}_4:\text{Mn}^{2+}$  emission is due to another reason. Actually the emission of beryllium-free  $\text{Zn}_2\text{SiO}_4:\text{Mn}^{2+}$  is narrow (Fig. 6.5). Let us, therefore, start with the latter phosphor which shows a bright-green emission.

Both  $\text{Zn}_2\text{SiO}_4$  and  $\text{Be}_2\text{SiO}_4$  have the phenacite structure with all metal ions in four coordination. The  $\text{Mn}^{2+}$  ( $3d^5$ ) ion has therefore also four coordination. All optical transitions within the  $3d^5$  configuration are spin- and parity forbidden (see Sect. 2.3.1). As a consequence excitation into these transitions does not yield a high light output. However, the luminescence of the  $\text{Mn}^{2+}$  ion in  $\text{Zn}_2\text{SiO}_4$  shows a strong excitation band in the 250 nm region which is probably due to a charge-transfer transition. Anyway, excitation into this band yields a high light output of the  $\text{Mn}^{2+}$  emission. The emission transition is  ${}^4\text{T}_1 \rightarrow {}^6\text{A}_1$ . The emission is relatively narrow, because the transition occurs within a given electron configuration (viz.  $3d^5$ ).

If we replace part of the  $\text{Zn}^{2+}$  ions by  $\text{Be}^{2+}$  ions, the crystal field on the  $\text{Mn}^{2+}$  ions will vary from ion to ion depending on the nature of the neighboring metal ions. This is due to the large difference between the ionic radii of  $\text{Zn}^{2+}$  and  $\text{Be}^{2+}$  (0.60 Å and 0.27 Å, respectively). Therefore, the emission band broadens relative to that of  $\text{Zn}_2\text{SiO}_4:\text{Mn}^{2+}$ . Obviously the introduction of  $\text{Be}^{2+}$  increases the crystal field on the  $\text{Mn}^{2+}$  ions, so that the emission shifts to longer wavelength (Fig. 2.10).

A serious drawback of this  $\text{Mn}^{2+}$  phosphor is its poor maintenance in a lamp. It easily picks up mercury from the gas discharge and is liable to decompose under ultraviolet radiation. In addition beryllium is highly toxic [7], and nowadays not acceptable for application. In 1948, these phosphors were replaced by one phosphor with blue and orange emission, viz.  $\text{Sb}^{3+}$ - and  $\text{Mn}^{2+}$ -activated calcium halophosphate.

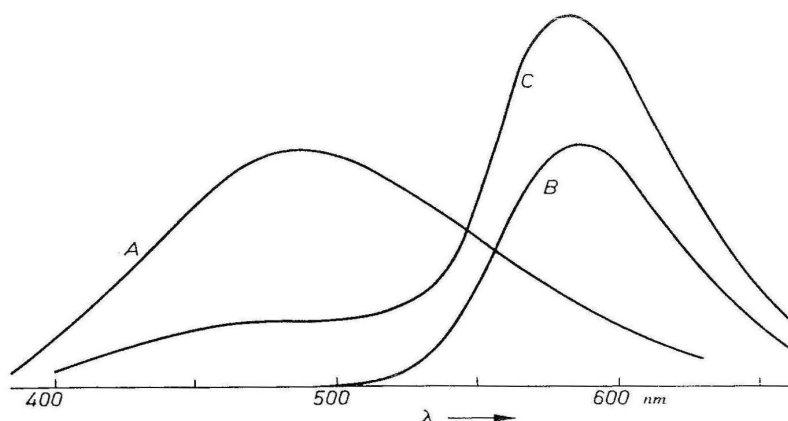


**Fig. 6.6.** Emission spectra of calcium halophosphates. A:  $\text{Sb}^{3+}$  emission; B:  $\text{Mn}^{2+}$  emission; C: warm-white halophosphate

#### 6.4.1.2 The Halophosphates [1-3]

The halophosphates with composition  $\text{Ca}_5(\text{PO}_4)_3\text{X}$  ( $\text{X} = \text{F}, \text{Cl}$ ) are closely related to hydroxy-apatite, the chief constituent of bones and teeth. The apatite crystal structure is hexagonal and offers two different sites for calcium, viz.  $\text{Ca}_\text{I}$  and  $\text{Ca}_\text{II}$ . The  $\text{Ca}_\text{I}$  sites form linear columns. Each  $\text{Ca}_\text{I}$  site is trigonally prismatic coordinated by six oxygen ions with average  $\text{Ca}_\text{I}-\text{O}$  distance 2.42 Å. Individual prisms share top and bottom. The sides of the prisms are capped by oxygen at a  $\text{Ca}_\text{I}-\text{O}$  distance of 2.80 Å, so that the total coordination is nine (by oxygen) and zero (by halogen). The  $\text{Ca}_\text{II}$  site has one halogen neighbour ( $\text{Ca}_\text{II}-\text{F}$ : 2.39 Å) and six oxygens (average  $\text{Ca}_\text{II}-\text{O}$ : 2.43 Å).

The optical absorption edge of the pure host lattice is at about 150 nm: all excitation energy from the mercury discharge has to be absorbed by the activators. Peculiarly enough, the crystallographic position of the  $\text{Sb}^{3+}$  and  $\text{Mn}^{2+}$  ions in this lattice is not exactly known. Optical and electron-paramagnetic-resonance data have shown that  $\text{Mn}^{2+}$  has a preference for the  $\text{Ca}_\text{I}$  site [8]. It is generally assumed that  $\text{Sb}^{3+}$  is on  $\text{Ca}_\text{II}$  sites with oxygen on the neighboring halogen site for charge compensation [8]:  $(\text{Sb}_{\text{Ca}}^{\bullet}, \text{O}_{\text{F}}^{\prime})^x$  in the Kröger notation [9]. However, this has been doubted by Mishra et al. [10], who suggest antimony on a phosphorus site with an oxygen vacancy for charge compensation:  $(\text{Sb}_{\text{P}}^{\bullet}, \text{V}_{\text{O}}^{\bullet\bullet})^x$ . This in turn has been questioned [11]. This situation shows that the apatite structure is a complicated one.

Jenkins et al. [12] discovered that  $\text{Sb}^{3+}$ -doped calcium halophosphate is a very efficient blue-emitting phosphor under 254 excitation (see Fig. 6.6). The  $\text{Sb}^{3+}$  ion has  $5s^2$  configuration and its  $^1\text{S}_0 \rightarrow ^3\text{P}_1$  and  $^1\text{P}_1$  absorption bands are situated at 255 and 205 nm, respectively (Fig. 6.7) [11]. The Stokes shift of the emission is enormous, viz.  $19\,000\text{ cm}^{-1}$  at room temperature.

These data teach us to become a little suspicious about the phantastic properties of the halophosphate phosphor. Excitation is into the  $^1\text{S}_0 \rightarrow ^3\text{P}_1$  transition. This is a spin-forbidden transition, and although it has a certain absorption strength by spin-orbit

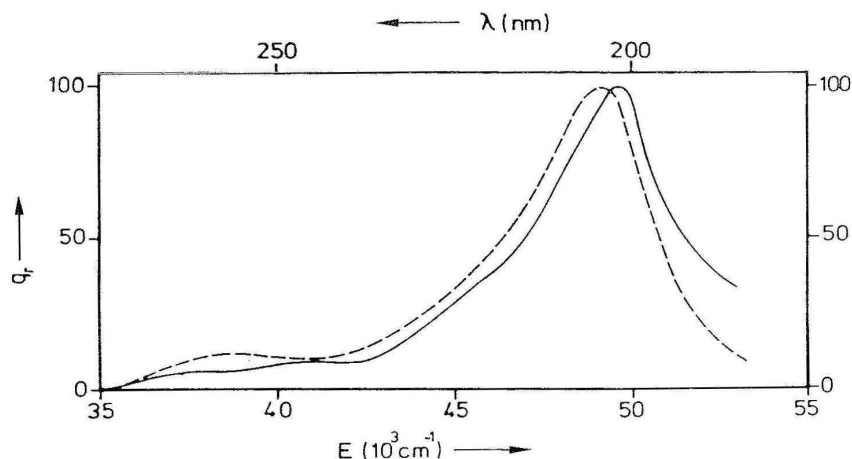


**Fig. 6.7.** Excitation spectrum of the  $\text{Sb}^{3+}$  emission of  $\text{Ca}_5(\text{PO}_4)_3\text{F}:\text{Sb}^{3+}$  at 4.2 K (continuous curve) and 290 K (broken curve)

coupling, it will never be as strongly absorbing as an allowed transition. Figure 6.7 shows this clearly, because the output for  $^1\text{S}_0 \rightarrow ^1\text{P}_1$  excitation is nearly an order of magnitude larger than for  $^1\text{S}_0 \rightarrow ^3\text{P}_1$  excitation (see also Sect. 2.3.5). In addition, the large Stokes shift predicts a low quantum efficiency (Sect. 4.2.2.). Actually  $q \simeq 70\%$  (Sect. 4.1). Such large Stokes shifts in case of  $s^2$  ions were discussed in Sect. 3.3.7.

When the halophosphate host lattice contains not only  $\text{Sb}^{3+}$  but also  $\text{Mn}^{2+}$ , part of the energy absorbed by the  $\text{Sb}^{3+}$  ions is transferred to  $\text{Mn}^{2+}$ . The  $\text{Mn}^{2+}$  ion shows an orange emission (see Fig. 6.6). The 254 nm radiation of the mercury discharge is hardly absorbed by the  $\text{Mn}^{2+}$  ions. The critical distance for energy transfer from  $\text{Sb}^{3+}$  to  $\text{Mn}^{2+}$  is about 10 Å; the acting mechanism is exchange [8]. This is not unexpected, since all optical transitions of the  $\text{Mn}^{2+}$  ion in the visible region are strongly forbidden (Sect. 5.2).

By carefully adjusting the ratio of the  $\text{Sb}^{3+}$  and  $\text{Mn}^{2+}$  ion concentrations, a white-emitting phosphor can be obtained with color temperatures ranging between 6500 and 2700 K. Figure 6.6 presents the emission spectrum of a warm-white halophosphate. A large drawback of the halophosphate lamps is the fact that it is impossible to have simultaneously high brightness and high color rendering: if the brightness is high (efficacy  $\sim 80$  lm/W), the color rendering index (CRI) is of the order of 60; the CRI value can be improved up to 90, but then the brightness decreases ( $\sim 50$  lm/W) [13]. The use of rare-earth activated phosphors has made it possible to achieve the combination of a high efficacy ( $\sim 100$  lm/W) with a high CRI value ( $\sim 85$ ).

#### 6.4.1.3 Phosphors for the Tricolor Lamp

It was predicted by Koedam and Opstelten [14] that a luminescent lamp with an efficacy of 100 lm/W and a CRI of 80-85 can be obtained by combining three phosphors which emit in narrow wavelength intervals centered around 450, 550 and 610 nm. A few years later such a lamp was realized using rare-earth activated phosphors [13]. This type of lamp is known as the tricolor lamp.

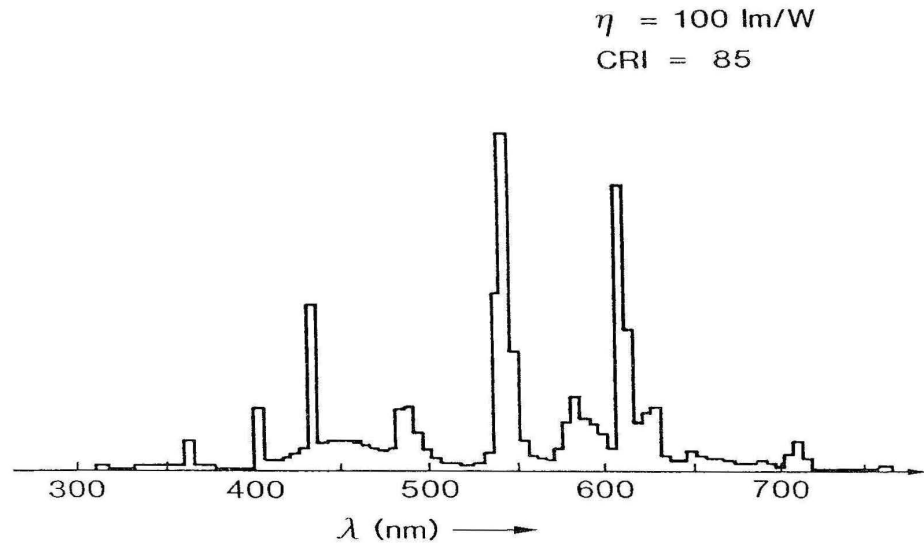


**Fig. 6.8.** Emission spectrum of a tricolor lamp with a color temperature of 4000 K. Reproduced with permission from Ref. [3]

As we have seen before, rare-earth ions can have narrow band or line emission (Chapters 2 and 3), and as a matter of fact  $\text{Eu}^{3+}$  is the best candidate for the red-emitting component and  $\text{Tb}^{3+}$  for the green-emitting component. They show line emission. For the blue the  $\text{Eu}^{2+}$  ion is taken with a narrow blue emission band, considerably narrower than the  $\text{Sb}^{3+}$  emission band.

The chromaticity diagram of Fig. 6.2 shows how white light can be obtained from the halophosphate phosphor by blending blue-green (BG) with orange (O), and how it can be obtained using three phosphors, i.e. by blending blue (B), green (G), and red (R). Figure 6.8 shows the emission spectrum of a tricolor lamp with a color temperature of 4000 K.

The individual phosphors for the tricolor lamp will now be discussed in separate sections.

#### 6.4.1.4 Red-Emitting Phosphors

The material  $\text{Y}_2\text{O}_3:\text{Eu}^{3+}$  fulfills all the requirements for a good red-emitting phosphor. Its emission is located at 613 nm and all other emission lines are weak. It can be easily excited by 254 nm radiation, and its quantum efficiency is high, viz. close to 100%.

The excitation of  $\text{Y}_2\text{O}_3:\text{Eu}^{3+}$  has already been discussed in Sect. 2.1: the 254 nm radiation is absorbed by the charge-transfer transition of the  $\text{Eu}^{3+}$  ion, the 185 nm radiation by the host lattice. Obviously the charge-transfer state is situated in the configurational coordinate diagram in such a way that it feeds the emitting levels exclusively (see Fig. 6.9). The emission spectrum of  $\text{Eu}^{3+}$  was discussed in Sect. 3.3.2.

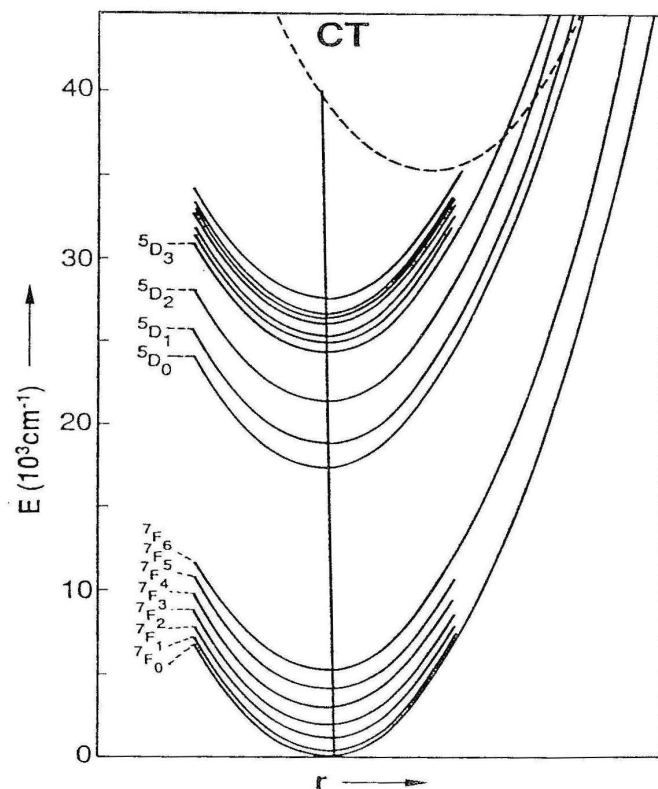


**Fig. 6.9.** Configuration coordinate diagram for  $\text{Eu}^{3+}$  in  $\text{Y}_2\text{O}_3$ . *CT*: charge-transfer state. Reproduced with permission from Ref. [38]

It consists of the  ${}^5\text{D}_0 - {}^7\text{F}_j$  line emissions with that to  $J = 2$  dominating due to its hypersensitivity (see Fig. 6.10).

However, the actual situation is more complicated. In the first place  $\text{Y}_2\text{O}_3$  offers two sites to the  $\text{Eu}^{3+}$  ion, one with  $\text{C}_2$  and one with  $\text{S}_6$  symmetry (see Fig. 6.11). There are three times more  $\text{C}_2$  sites, and  $\text{Eu}^{3+}$  is assumed to occupy these two types of sites in a statistical way. The  $\text{S}_6$  site has inversion symmetry, so that the  $\text{Eu}^{3+}$  ion on this site will only show the  ${}^5\text{D}_0 - {}^7\text{F}_1$  magnetic-dipole emission (Sect. 3.3.2) which is situated around 595 nm. The strongly forbidden character of the  ${}^5\text{D}_0 - {}^7\text{F}_j$  transitions of  $\text{Eu}^{3+}(\text{S}_6)$  becomes clear from the value of the decay time of 8 ms compared with 1.1 ms for  $\text{Eu}^{3+}(\text{C}_2)$  [15].

The unwanted  ${}^5\text{D}_0 - {}^7\text{F}_1$  emission of the  $\text{S}_6$  site is suppressed in the commercial 3%  $\text{Eu}^{3+}$  samples by the occurrence of energy transfer from  $\text{Eu}^{3+}(\text{S}_6)$  to  $\text{Eu}^{3+}(\text{C}_2)$ . The critical distance for this transfer amounts to about 8 Å and exchange as well as dipole-quadrupole interaction seem to play a role [15].

Other advantages of the 3% concentration are the quenching of the unwanted higher level emission from  $\text{Eu}^{3+}$  (i.e.  ${}^5\text{D}_j - {}^7\text{F}_j$ ,  $J > 0$ ; see Sect. 5.3) by cross-relaxation,

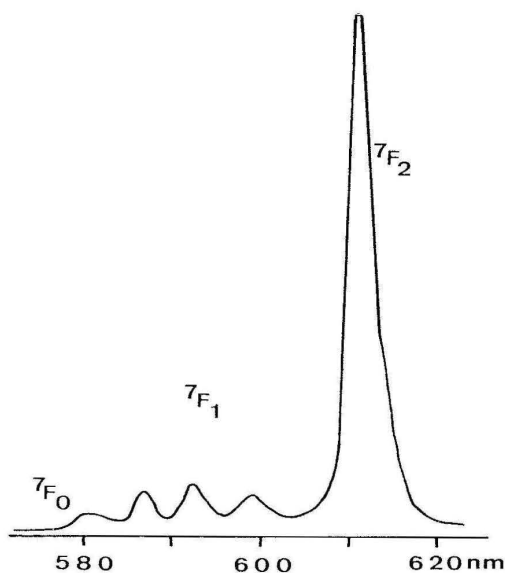


**Fig. 6.10.** Emission spectrum of  $Y_2O_3:Eu^{3+}$ . The final levels of the  $^5D_0 - ^7F_J$  transitions are indicated

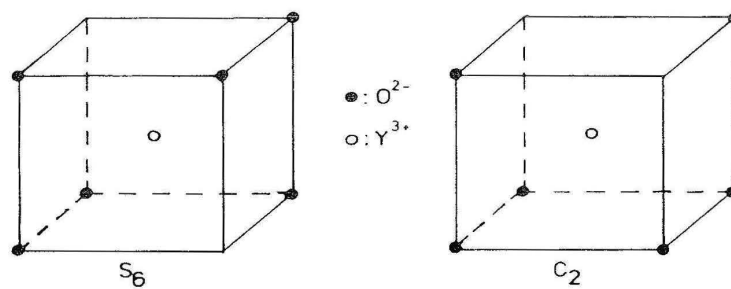


**Fig. 6.11.** Oxygen surroundings of  $Y^{3+}$  ( $Eu^{3+}$ ) in  $Y_2O_3:Eu^{3+}$ . On the left hand side is the  $S_6$  site with inversion symmetry, on the right hand side the  $C_2$  site

and a sufficient absorption strength of the 254 nm radiation. On the other hand the high europium concentration makes the phosphor very expensive, especially since high purity  $Y_2O_3$  is required which is also not cheap. Impurities in  $Y_2O_3$  tend to act as competing absorbing centers, i.e. they absorb the 254 nm radiation without converting it into visible light. A serious impurity is iron. It has been estimated that 5 ppm Fe lowers the quantum efficiency by 7% [16]. Below we will discuss research performed in order to lower the price of the red-emitting phosphor.



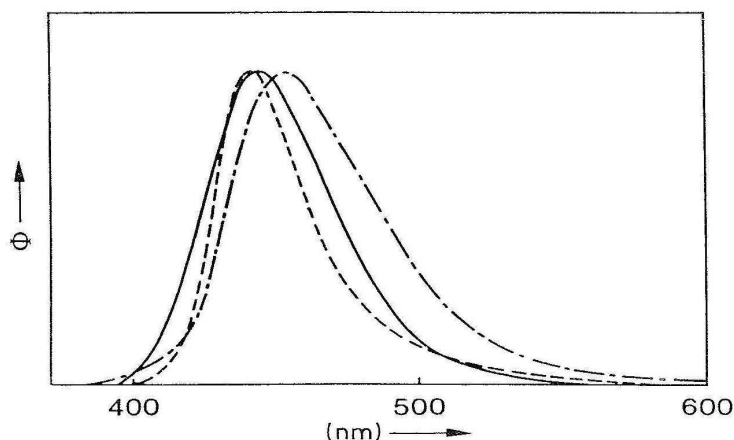


**Fig. 6.12.** Emission spectra of three blue-emitting  $\text{Eu}^{2+}$  phosphors. Full line:  $\text{BaMgAl}_{10}\text{O}_{17}:\text{Eu}^{2+}$ ; broken line:  $\text{Sr}_5(\text{PO}_4)_3\text{Cl}:\text{Eu}^{2+}$ ; broken line with dots:  $\text{Sr}_2\text{Al}_6\text{O}_{11}:\text{Eu}^{2+}$ . Reproduced with permission from Ref. [3]

#### 6.4.1.5 Blue-Emitting Phosphors

The highest lamp output is expected for a blue-emitting phosphor with an emission maximum at 450 nm, whereas the best CRI is found with an emission maximum at 480 nm. Since the tricolor lamp aims at high light output in combination with good color rendition, only phosphors with an emission maximum between 440 and 460 nm are of practical interest. Figure 6.12 shows the emission spectrum of three  $\text{Eu}^{2+}$ -activated phosphors which satisfy the requirements:  $\text{BaMgAl}_{10}\text{O}_{17}:\text{Eu}^{2+}$ ,  $\text{Sr}_3(\text{PO}_4)_5\text{Cl}:\text{Eu}^{2+}$ , and  $\text{Sr}_2\text{Al}_6\text{O}_{11}:\text{Eu}^{2+}$  [3]. Their quantum efficiencies are about 90%. The spectroscopy of the  $\text{Eu}^{2+}$  ion was treated in Sect. 3.3.3b.

The compound  $\text{BaMgAl}_{10}\text{O}_{17}$  has a crystal structure related to the magnetoplumbite structure. This structure consists of spinel layers with interlayers containing  $\text{Ba}^{2+}$ . The complicated nature of this composition is illustrated by the fact that originally it was written as “ $\text{BaMg}_2\text{Al}_{16}\text{O}_{27}$ ” [13]. The situation has been discussed by Smets et al. [17].

The compound  $\text{Sr}_5(\text{PO}_4)_3\text{Cl}$  belongs to the halophosphates mentioned above, whereas  $\text{Sr}_2\text{Al}_6\text{O}_{11}$  is built up of alternating layers of  $\text{AlO}_4$  tetrahedra and of  $\text{AlO}_6$  octahedra [18]. The structure is shown schematically in Fig. 6.13.

#### 6.4.1.6 Green-Emitting Phosphors

The green-emitting ion in the tricolor lamp is  $\text{Tb}^{3+}$ . Its first allowed absorption band is  $4f^8 \rightarrow 4f^75d$  (Sect. 2.3.4.). It often lies at too high energy to make 254 nm excitation effective. In order to absorb the 254 nm radiation efficiently, a sensitizer has to be used. For this purpose the  $\text{Ce}^{3+}$  ion is very suitable. Its  $4f \rightarrow 5d$  transition is situated at lower energy than the corresponding  $4f^8 \rightarrow 4f^75d$  transition of  $\text{Tb}^{3+}$ . Table 6.1

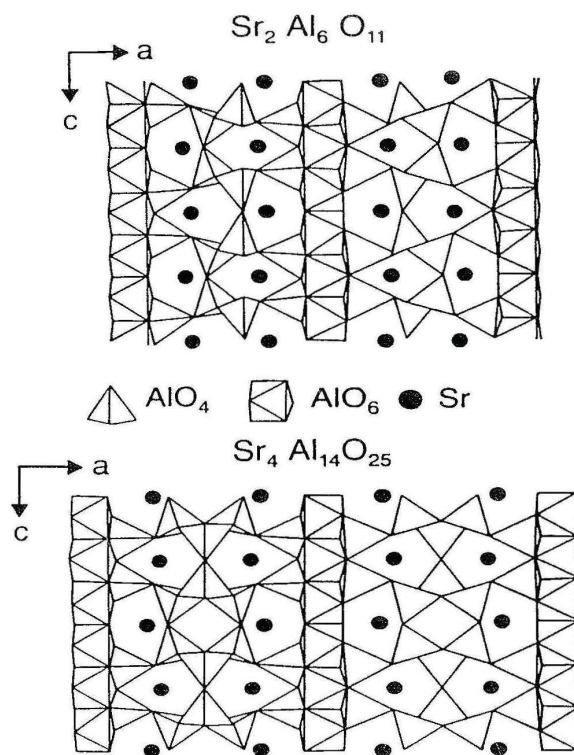


**Fig. 6.13.** Crystal structures of  $\text{Sr}_2\text{Al}_6\text{O}_{11}$  and  $\text{Sr}_4\text{Al}_{14}\text{O}_{25}$ . Reproduced with permission from Ref. [3]

**Table 6.1.** Quantum efficiency  $q$  for ultraviolet (UV) and visible (VIS) emission for 254 nm excitation of green phosphors applied in the tricolor lamp [3].

Composition	$q_{\text{UV}}$ (%)	$q_{\text{VIS}}$ (%)
$\text{Ce}_{0.67}\text{Tb}_{0.33}\text{MgAl}_{11}\text{O}_{19}$	5	85
$\text{Ce}_{0.45}\text{La}_{0.40}\text{Tb}_{0.15}\text{PO}_4$	7	86
$\text{Ce}_{0.3}\text{Gd}_{0.5}\text{Tb}_{0.2}\text{MgB}_5\text{O}_{10}$	2	88

shows the green phosphors in use, with their chemical composition and quantum efficiencies in the ultraviolet and visible.

The host lattice  $\text{CeMgAl}_{11}\text{O}_{17}$  has the magnetoplumbite structure,  $\text{LaPO}_4$  the monazite structure, and  $\text{GdMgB}_5\text{O}_{10}$  a structure consisting of a two-dimensional framework of  $\text{BO}_3$  and  $\text{BO}_4$  groups in which the  $\text{Mg}^{2+}$  ions are in octahedral coordination and  $\text{Gd}^{3+}$  in ten coordination [19]. The  $\text{Gd}^{3+}$  polyhedra form isolated zig-zag chains. The shortest Gd–Gd intrachain distance is about 4 Å, the shortest Gd–Gd interchain distance 6.4 Å.

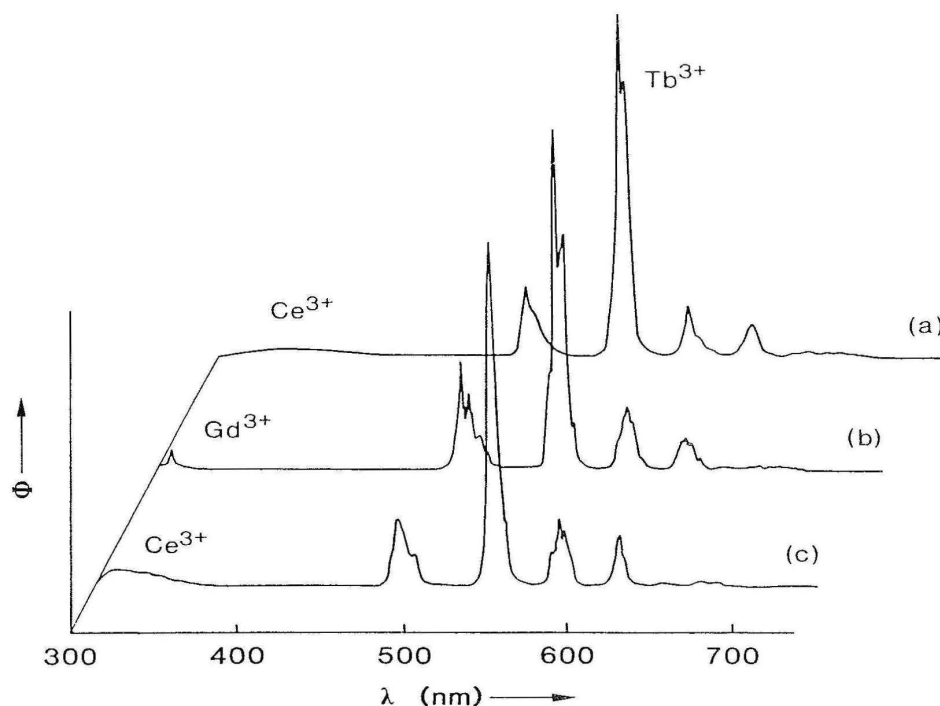


**Fig. 6.14.** Emission spectra of three green-emitting  $\text{Tb}^{3+}$  phosphors. (a):  $\text{CeMgAl}_{11}\text{O}_{19}:\text{Tb}^{3+}$ ; (b):  $(\text{Ce,Gd})\text{MgB}_5\text{O}_{10}:\text{Tb}^{3+}$ ; (c):  $(\text{La,Ce})\text{PO}_4:\text{Tb}^{3+}$ . Reproduced with permission from Ref. [3]

Figure 6.14 shows the emission spectra of the three green phosphors. In all of them some ultraviolet emission originating from  $\text{Ce}^{3+}$  or  $\text{Gd}^{3+}$  is present. The energy transfer phenomena are different as will be discussed now.

The  $\text{Ce}^{3+}$  emission of  $\text{CeMgAl}_{11}\text{O}_{19}$  has its emission maximum at 330 nm and the first excitation maximum at 270 nm, so that the Stokes shift is large ( $\sim 8000 \text{ cm}^{-1}$ ) [20]; energy transfer between  $\text{Ce}^{3+}$  ions does not occur and concentration quenching is absent. The  $\text{Ce}^{3+} \rightarrow \text{Tb}^{3+}$  transfer is a one-step transfer process. Since this transfer is restricted to neighbors due to the forbidden nature of the intraconfigurational  $4f^8$  transitions on  $\text{Tb}^{3+}$ , high  $\text{Tb}^{3+}$  concentrations are necessary to quench the  $\text{Ce}^{3+}$  emission. Even 33% Tb is not able to do so completely (see Table 6.1).

In  $(\text{La,Ce})\text{PO}_4$  the Stokes shift of the emission is smaller ( $\sim 6000 \text{ cm}^{-1}$ ), and the emission of  $\text{CePO}_4$  is partly concentration quenched. Energy migration over the  $\text{Ce}^{3+}$  ions assists in the transfer to  $\text{Tb}^{3+}$  and less  $\text{Tb}^{3+}$  is needed. Nevertheless the UV output is relatively high (see Table 6.1). This is due to the fact that the  $\text{Ce}^{3+}-\text{Ce}^{3+}$  transfer is more efficient than the  $\text{Ce}^{3+}-\text{Tb}^{3+}$  transfer. At the shortest internuclear rare-earth distance the transfer rates amount to  $10^{11}\text{s}^{-1}$  and  $3 \times 10^8\text{s}^{-1}$ , respectively. This phosphor system has been discussed at length recently [21].

In  $\text{GdMgB}_5\text{O}_{10}:\text{Ce}^{3+},\text{Tb}^{3+}$  the situation is even more complicated. Excitation with 254 nm radiation occurs in the  $\text{Ce}^{3+}$  ion which transfers its energy to the  $\text{Gd}^{3+}$  ions.

**Table 6.2.** Energytransfer processes in the green phosphors for the tricolor lamp.

Phosphor	Energy transfer processes
CeMgAl <sub>11</sub> O <sub>19</sub> :Tb	Ce <sup>3+</sup> → Tb <sup>3+</sup>
LaPO <sub>4</sub> :Ce,Tb	Ce <sup>3+</sup> → Ce <sup>3+</sup> *
	Ce <sup>3+</sup> → Tb <sup>3+</sup>
GdMgB <sub>5</sub> O <sub>10</sub> :Ce, Tb	Ce <sup>3+</sup> → Gd <sup>3+</sup>
	Gd <sup>3+</sup> → Gd <sup>3+</sup> *
	Gd <sup>3+</sup> → Tb <sup>3+</sup>

\* This transfer occurs many times repeatedly.

In order to have efficient transfer, the Ce<sup>3+</sup> emission in the absence of Gd<sup>3+</sup> must be situated at about 280 nm which makes transfer to the 6<sub>1</sub> levels of Gd<sup>3+</sup> possible. This restricts the Stokes shift of the Ce<sup>3+</sup> emission to some 4000 cm<sup>-1</sup>. This has been observed in a few cases only, because not only the Stokes shift should be small, but also the first absorption transition of the Ce<sup>3+</sup> ion should be at relatively high energy, requiring an ionic host lattice (see Sect. 2.2). Host lattices which satisfy these requirements are GdB<sub>3</sub>O<sub>6</sub>, GdF<sub>3</sub>, NaGdF<sub>4</sub> (but not LiGdF<sub>4</sub>) and GdMgB<sub>5</sub>O<sub>10</sub> [22]. If the Ce<sup>3+</sup> levels shift to somewhat lower energy (for example in Li<sub>6</sub>Gd(BO<sub>3</sub>)<sub>3</sub>:Ce<sup>3+</sup>), the transfer occurs only in the opposite direction, i.e. from Gd<sup>3+</sup> to Ce<sup>3+</sup>. Other ions can also be used as sensitizer of the Gd<sup>3+</sup> sublattice viz. Pr<sup>3+</sup>, Pb<sup>2+</sup>, Bi<sup>3+</sup> [22].

In GdMgB<sub>5</sub>O<sub>10</sub>:Ce,Tb practically all Ce<sup>3+</sup> excitation energy is transferred to the Gd<sup>3+</sup> ions. Subsequently, the energy migrates over the Gd<sup>3+</sup> sublattice (see Sect. 5.3). It is trapped by the emitting Tb<sup>3+</sup> ions. Care should be taken that the energy is not trapped by impurity ions which act as killers. Their role can be overruled by using a high Tb<sup>3+</sup> concentration.

Finally we note that the energy migration over the Gd<sup>3+</sup> sublattice seems to be less one-dimensional than the crystal structure suggests [23]. Table 6.1 shows that the use of Gd<sup>3+</sup> host lattices makes it possible to convert more ultraviolet radiation into visible light. Table 6.2 summarizes the energy transfer processes in the green phosphors considered above.

#### 6.4.1.7 Phosphors for Special Deluxe Lamps

Tricolor lamps show only emission in restricted wavelength intervals. For objects with a reflection spectrum peaking outside these regions the color appearance under illumination with a tricolor lamp will differ from the one under illumination with a black body radiator. Although a CRI of 85 guarantees a normal appearance for most objects, some typical colors will look unnatural under illumination with a tricolor lamp. For certain applications, therefore, a higher CRI is required. Examples of such applications are museum illumination and flower displays. For this purpose special deluxe lamps were developed with a CRI of 95. Simultaneously we have to accept an efficacy drop to 65 lm/W [3].

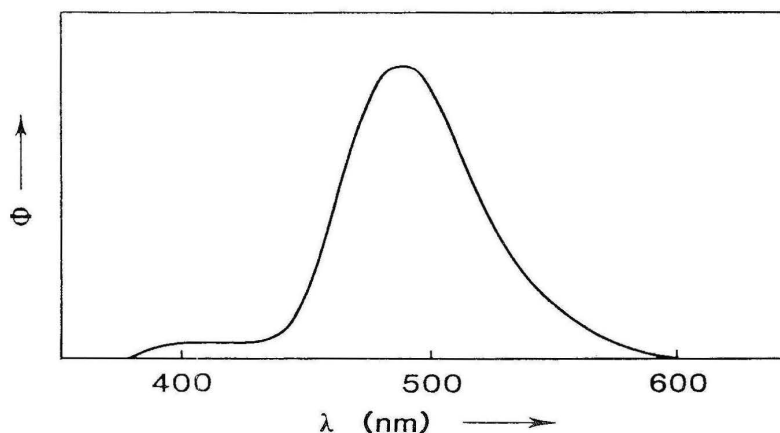


**Fig. 6.15.** Emission spectrum of  $\text{Sr}_4\text{Al}_{14}\text{O}_{25} : \text{Eu}^{2+}$

As pointed out above (Sect. 6.4.1.5), a higher CRI can be obtained by using a blue-emitting phosphor with an emission maximum at 490 nm. A further increase of the CRI can be obtained by using band instead of line phosphors for the red and green. In this way a more or less continuous spectrum extending from the blue to the red is obtained.

A suitable blue emission is given by  $\text{Sr}_4\text{Al}_{14}\text{O}_{25} : \text{Eu}^{2+}$  with an emission maximum at 490 nm (see Fig. 6.15) and a quantum efficiency of 90%. The crystal structure of  $\text{Sr}_4\text{Al}_{14}\text{O}_{25}$  is given in Fig. 6.13 and is related to that of  $\text{Sr}_2\text{Al}_6\text{O}_{11}$  [3]. In addition to the 490 nm emission band there is a weak emission band at 410 nm. This is due to the presence of two different crystallographic sites for Sr in  $\text{Sr}_4\text{Al}_{14}\text{O}_{25}$ , so that there are also two types of  $\text{Eu}^{2+}$  ions. Although both sites have the same abundance, the 490 nm emission is by far the dominating emission. This favourable situation is due to efficient energy transfer from the 410 nm emitting  $\text{Eu}^{2+}$  ion to the 490 nm emitting  $\text{Eu}^{2+}$  ion. There is a large spectral overlap between the 410 nm emission band and the excitation band of the 490 nm emitting  $\text{Eu}^{2+}$  ion, and all optical transitions involved ( $4f^7 \leftrightarrow 4f^65d$ ) are allowed. Therefore all conditions for efficient energy transfer are fulfilled (compare Sect. 5.2). A critical distance of some 35 Å has been found [24].

A broad-band red-emitting phosphor has been obtained in the host lattice  $\text{GdMgB}_5\text{O}_{10}$ . Again  $\text{Ce}^{3+}$  is used as a sensitizer, but this time  $\text{Mn}^{2+}$  as an activator. The  $\text{Mn}^{2+}$  ion on  $\text{Mg}^{2+}$  sites, i.e. in octahedral coordination, yields a red emission peaking around 630 nm. This emission corresponds to the  ${}^4\text{T}_1 \rightarrow {}^6\text{A}_1$  transition (Sect. 3.3.4.c). The transfer to  $\text{Mn}^{2+}$  occurs via the  $\text{Gd}^{3+}$  sublattice as described above (Sect. 6.4.1.6). By using a composition  $\text{Ce}_{0.2}\text{Gd}_{0.6}\text{Tb}_{0.2}\text{Mg}_{0.9}\text{Mn}_{0.1}\text{B}_5\text{O}_{10}$  a phosphor is obtained which emits simultaneously green and red.

An efficient broad-band green-emitting phosphor is not known, but can be simulated by combining  $\text{Tb}^{3+}$  emission with the  $\text{Mn}^{2+}$  emission of the halophosphate phosphor. A lamp containing a mixture of  $\text{Sr}_2\text{Al}_6\text{O}_{11} : \text{Eu}^{2+}$ ,  $\text{GdMgB}_5\text{O}_{10} : \text{Ce}^{3+}, \text{Tb}^{3+}, \text{Mn}^{2+}$  and  $\text{Ca}_5(\text{PO}_4)_3(\text{F}, \text{Cl}) : \text{Sb}^{3+}, \text{Mn}^{2+}$  has a CRI of 95 and an efficacy of 65 lm/W. Its emission spectrum is shown in Fig. 6.16.

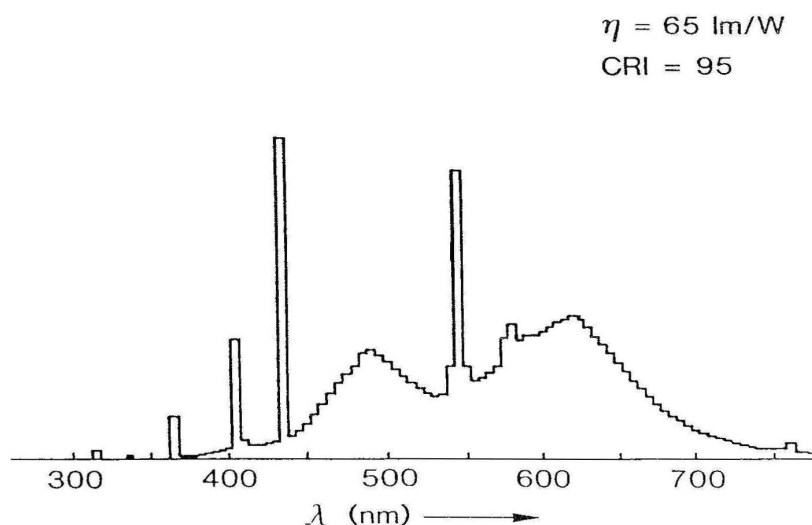


**Fig. 6.16.** Emission spectrum of a Special Deluxe lamp with a color temperature of 4000 K. Reproduced with permission from Ref. [3]

Figure 6.16 shows on the short wavelength side the blue mercury lines. These can be efficiently suppressed by adding  $\text{Y}_3\text{Al}_5\text{O}_{12}:\text{Ce}^{3+}$ . This phosphor, with garnet structure, absorbs blue light and converts it with high efficiency into yellow emission (see Fig. 6.17). The optical transitions involved are due to  $\text{Ce}^{3+}$ . In the garnet structure this ion undergoes such a strong crystal field, that the lowest  $4f \rightarrow 5d$  transition is in the visible (Sect. 2.3.4). A comparison of  $\text{Ce}^{3+}$  in  $\text{Y}_3\text{Al}_5\text{O}_{12}$  with  $\text{Ce}^{3+}$  in  $\text{GdMgB}_5\text{O}_{10}$  (Sect. 6.4.1.6) illustrates how large the influence of the host lattice on the energy levels of a luminescent ion may be.

#### 6.4.1.8 The Maintenance of Phosphors in Tricolor Lamps

The phosphors in the tricolor lamp show another advantage over the halophosphate phosphors, viz. a much better maintenance during lamp life. In Fig. 6.18 the output decrease after 2000 hours of burning is plotted as a function of the wall load. The higher stability of the rare-earth activated phosphors is translated into a higher maintenance. The value of the wall load is determined by the tube diameter (see Fig. 6.18). Tricolor and Special Deluxe lamps are now available in a tube diameter of 25 mm, to be compared with the 36 mm of the halophosphate tube. It even proved to be possible to reduce the tube diameter to 10 mm. With this small diameter the discharge tube can be fold up and the compact luminescent lamp is born.

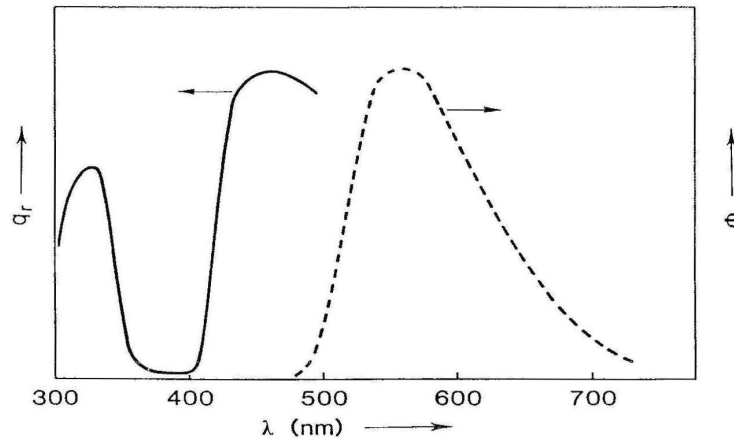


**Fig. 6.17.** Emission (dashed line) and excitation (continuous line) spectra of the luminescence of  $\text{Y}_3\text{Al}_5\text{O}_{12}:\text{Ce}^{3+}$

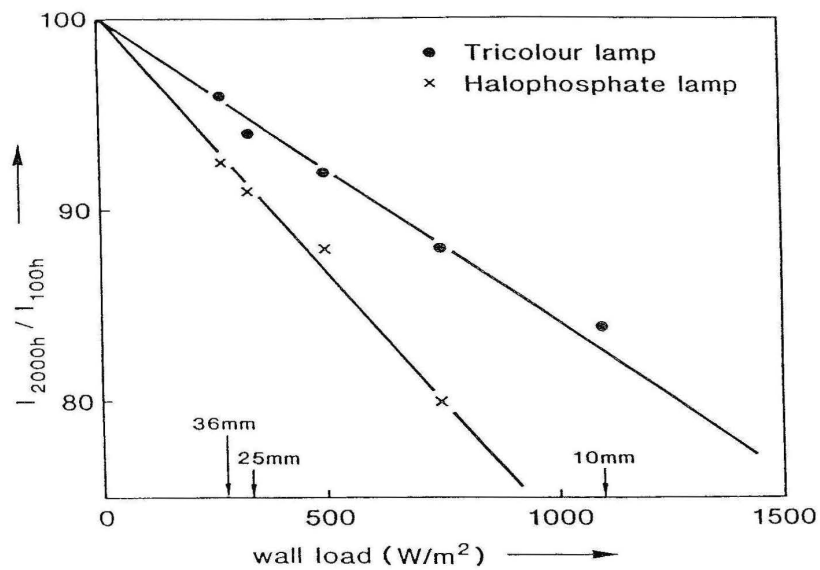


**Fig. 6.18.** Ratio of the lamp outputs after 2000 and 100 hours of burning as a function of the wall load. Crosses are for a halophosphate lamp, circles for a tricolor lamp. Commercial lamp diameters are indicated. Reproduced with permission from Ref. [3]

### 6.4.2 Phosphors for Other Lamp Applications

Low-pressure mercury discharge lamps are not only used for lighting. Since it is in principle possible to have a phosphor with every wavelength desired, there are many, more specialized applications. Here we mention a few.

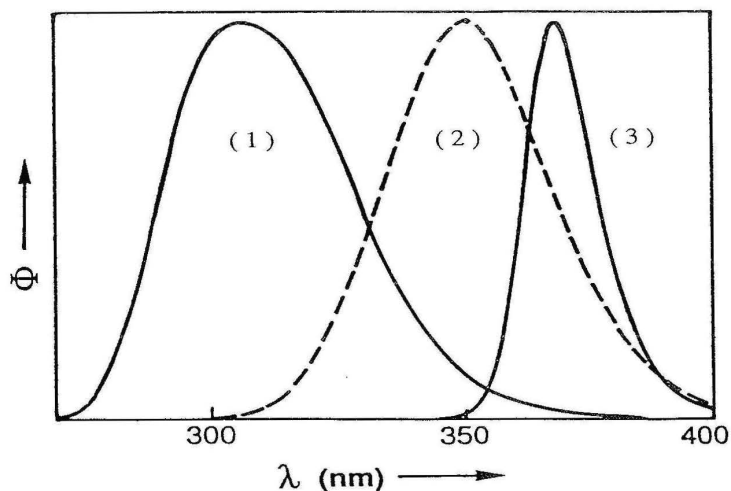


**Fig. 6.19.** Emission spectra of several ultraviolet-emitting phosphors. (1):  $\text{SrAl}_{12}\text{O}_{19}:\text{Ce}^{3+}, \text{Mg}^{2+}$ ; (2):  $\text{BaSi}_2\text{O}_5:\text{Pb}^{2+}$ ; (3):  $\text{SrB}_4\text{O}_7:\text{Eu}^{2+}$

In phototherapy the emission of the lamp should correspond to the stimulation spectrum of the human skin. For  $\lambda < \sim 300$  nm sunburn (erythema) occurs, and for  $\lambda > 330$  nm direct pigmentation (skin darkening) occurs, but this disappears after a short time [3]. In the intermediate range delayed pigmentation (melanin production) occurs yielding a long lasting tan. Figure 6.19 shows the emission spectra of three ultraviolet-emitting phosphors.

It is clear that  $\text{SrAl}_{12}\text{O}_{19}:\text{Ce}^{3+}, \text{Mg}^{2+}$  (with magnetoplumbite structure and  $\text{Ce}^{3+}$  on  $\text{Sr}^{2+}$  sites and  $\text{Mg}^{2+}$  on  $\text{Al}^{3+}$  sites for charge compensation) will induce severe sunburn. On the other hand  $\text{SrB}_4\text{O}_7:\text{Eu}^{2+}$ , discussed in Sect. 3.3.3b, will induce only direct pigmentation. For a long lasting tan it is necessary to use lamps with  $\text{BaSi}_2\text{O}_5:\text{Pb}^{2+}$ . Considerations of this type are of importance in the development of sun-tanning lamps.

The  $\text{Gd}^{3+}$  emission is used in lamps to control psoriasis [3]. This skin disease cannot be cured, but by using ultraviolet treatment it can be controlled. The 312 nm emission of  $\text{Gd}^{3+}$  controls effectively the spread of psoriasis without too much sunburn. However, the  $\text{Gd}^{3+}$  ion cannot be excited directly with 254 nm radiation, since all optical transitions within its  $4f^7$  configuration are strongly forbidden and the excited  $4f^65d$  configuration is at very high energy ( $> 70\,000\text{ cm}^{-1}$ ). Therefore it is necessary to use a sensitizer. For these lamps  $\text{GdBO}_3:\text{Pr}^{3+}$  or  $(\text{La}, \text{Gd})\text{B}_3\text{O}_6:\text{Bi}^{3+}$  can be used [3].

In  $\text{GdBO}_3:\text{Pr}^{3+}$  the 254 nm excitation is absorbed by  $\text{Pr}^{3+}$  ( $4f^2 \rightarrow 4f5d$ ). After relaxation the  $\text{Pr}^{3+}$  ion transfers its excitation energy to  $\text{Gd}^{3+}$ . Energy migration over the  $\text{Gd}^{3+}$  sublattice follows. Since the  $\text{Pr}^{3+}$  ion has no energy levels coinciding with the lowest excited level of the  $\text{Gd}^{3+}$  ion, the excitation energy is emitted by  $\text{Gd}^{3+}$  itself. This is shown schematically in Fig. 6.20.



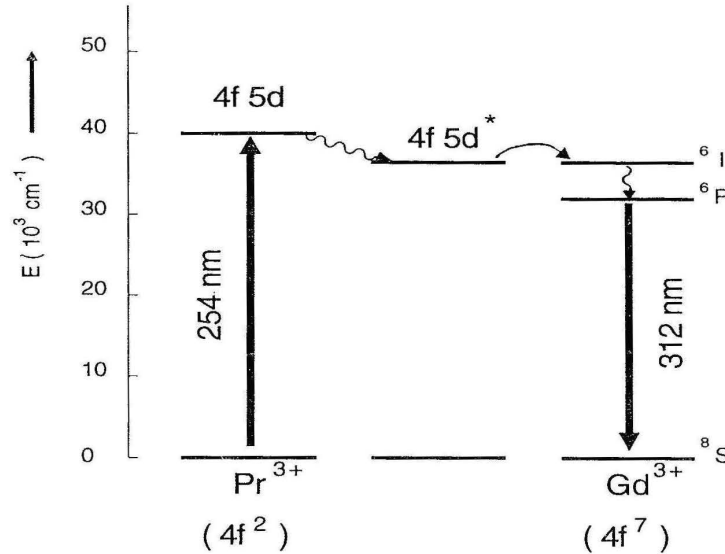


**Fig. 6.20.** The luminescence of  $\text{GdBO}_3:\text{Pr}^{3+}$ . Excitation is into the  $4f^2 \rightarrow 4f5d$  transition of  $\text{Pr}^{3+}$ , which ion transfers to the  $\text{Gd}^{3+}$  ion, which emits its  ${}^6\text{P}$  emission. The level  $4f5d^*$  indicates the relaxed excited state of  $\text{Pr}^{3+}$ . Energy migration over the  $\text{Gd}^{3+}$  sublattice is omitted for simplicity

In  $(\text{La,Gd})\text{B}_3\text{O}_6:\text{Bi}^{3+}$  the transfer phenomena are similar. The  $\text{Bi}^{3+}$  ion ( $6s^2$  configuration) absorbs the 254 nm radiation in the  ${}^1\text{S}_0 \rightarrow {}^3\text{P}_1$  transition (Sect. 2.3.5). The relaxed  ${}^3\text{P}_1$  state transfers this excitation energy to the  $\text{Gd}^{3+}$  ion from which emission occurs.

Further, blue-emitting  $\text{Sr}_2\text{P}_2\text{O}_7:\text{Eu}^{2+}$ , with an emission maximum at 420 nm and  $q \sim 90\%$ , can be used in lamps in the phototherapy of hyperbilirubinemia (an excess of bilirubin in the blood serum which may result in permanent brain damage in newborn infants).

### 6.4.3 Phosphors for High-Pressure Mercury Vapour Lamps

Phosphors for this application should have a red emission which can be excited by long- as well as short-wavelength ultraviolet radiation with high quantum efficiency up to  $300^\circ\text{C}$  (see Sect. 6.2). Here we mention three different phosphors which can be used, viz. magnesium(fluoro) germanate doped with  $\text{Mn}^{4+}$ ,  $(\text{Sr,Mg})_3(\text{PO}_4)_2:\text{Sn}^{2+}$ , and (modified)  $\text{YVO}_4:\text{Eu}^{3+}$ .

The formula of the first host lattice has been given as  $\text{Mg}_{28}\text{Ge}_{7.5}\text{O}_{38}\text{F}_{10}$ . The  $\text{Mn}^{4+}$  ion ( $3d^3$  configuration) absorbs over the whole ultraviolet range with an intense charge-transfer transition. The emission is in the deep red (620–670 nm), consists of several lines, and is due to the  ${}^2\text{E} \rightarrow {}^4\text{A}_2$  transition (Sect. 3.3.4b). Thermal quenching occurs only above  $300^\circ\text{C}$  as is to be expected for a narrow line emission. The decay

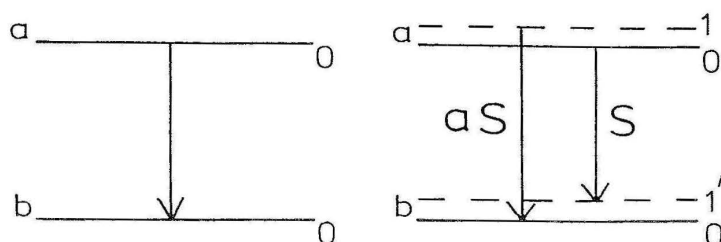
**Table 6.3.** Emission lines of the  $\text{Mn}^{4+}$  activated fluorogermanate [2] and their assignment (see also Fig. 6.22).

Spectral position		Assignment (values in $\text{cm}^{-1}$ )
nm	$\text{cm}^{-1}$	
626.2 <sup>a</sup>	15.969 <sup>a</sup>	$0 - 0 + 405 (\nu_4)$ b
632.5 <sup>a</sup>	15.810 <sup>a</sup>	$0 - 0 + 246 (\nu_3)$ c
642.5	15.564	$0 - 0$
652.5	15.326	$0 - 0 - 238 (\nu_3)$ c
660.0	15.152	$0 - 0 - 412 (\nu_4)$ b
670.0	14.925	$0 - 0 - 639 (\nu_1?)$

a lacking at 77 K

b intensity ratio of anti-Stokes and Stokes lines at 300 K amounts to 0.1 (experimental) and 0.13 (calculated).

c intensity ratio 0.4 (exp.) and 0.30 (calc.)

**Fig. 6.21.** Schematic representation of a zero-phonon transition (left-hand side), and the Stokes (*S*) and anti-Stokes (*aS*) vibronic transitions (right-hand side) in emission. Lettering refers to electronic states, numbering to vibrational states

time is long, viz.  $\sim 3.5$  ms, as is to be expected for a spin- and parity-forbidden transition.

Since the spectroscopy of this phosphor is incorrectly described in the book on lamp phosphors [2], we add here, also as an illustration of the theory, a few comments on the spectroscopy. In view of its electron configuration ( $d^3$ ), the  $\text{Mn}^{4+}$  ion will be octahedrally coordinated. The emission lines are tabulated in Table 6.3. There is a zero-phonon transition (Sect. 2.1) which at low temperatures is followed by vibronic lines due to coupling with the asymmetric  $\text{Mn}^{4+}-\text{O}^{2-}$  deformation and stretching modes,  $\nu_4$  and  $\nu_3$ , respectively. These uneven modes relax the parity selection rule. At room temperature there occur also anti-Stokes vibronics (Figs. 6.21 and 6.22). The vibrational modes in the excited state and ground state are equal within the experimental accuracy as is to be expected for the narrow  ${}^2\text{E} \rightarrow {}^4\text{A}_2$  transition [25,26]. The intensity ratio of the Stokes and anti-Stokes vibronic lines agrees with the Bose-Einstein distribution [26].

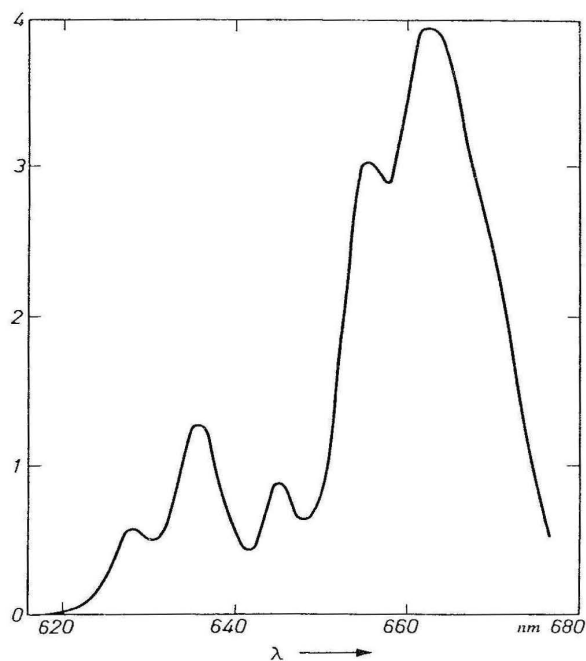


**Fig. 6.22.** Emission spectrum of  $\text{Mn}^{4+}$ -activated magnesium fluorogermanate

As argued in Sect. 4.2, the position of the charge-transfer state determines the quenching temperature. In the present case this means that the  ${}^2\text{E}$  level will decay nonradiatively via the charge-transfer state. This has been suggested before in a discussion of the  $\text{Mn}^{4+}$  emission in  $\text{CaZrO}_3$  [27]. In this composition the charge-transfer state is at  $30\,000\text{ cm}^{-1}$ , yielding a quenching temperature of 300 K. In the fluorogermanate these values are  $35\,000\text{ cm}^{-1}$  and 700 K, respectively. This illustrates how important the position of the charge-transfer state is for efficient luminescence.

Butler [2] has shown that, when carefully prepared,  $\text{Sn}^{2+}$ -activated phosphors can be efficient phosphors. For example,  $(\text{Sr},\text{Mg})_3(\text{PO}_4)_2 : \text{Sn}^{2+}$  shows a broad-band red emission with a maximum at about 630 nm and a thermal quenching which starts above  $300^\circ\text{C}$ . The  $\text{Sn}^{2+}$  ion has  $5s^2$  configuration, but its luminescence is not so simple as the discussion in Sect. 3.3.7 may suggest. For example, it is not easy to understand why the emission is so far in the visible, whereas in many other host lattices it is in the ultraviolet or blue. Donker et al. have found that the coordination number is of critical influence: high coordination yields ultraviolet or blue emission, low coordination yellow or red emission [28].

Of a more recent date are compositions based on  $\text{YVO}_4 : \text{Eu}^{3+}$  which was originally introduced as the red primary in color television tubes (see Chapter 7) [29]. This is a very interesting phosphor material. It absorbs the greater part of the ultraviolet spectrum in the  $\text{VO}_4^{3-}$  group. By energy migration over the vanadate groups the  $\text{Eu}^{3+}$  ion is reached (Sect. 5.3.2). The  $\text{Eu}^{3+}$  ion shows in  $\text{YVO}_4$  relatively-red emission lines ( ${}^5\text{D}_0 - {}^7\text{F}_2$  emission transitions at 614 and 619 nm), and thermal quenching

occurs only above 300°C [30]. The thermal quenching is due to the fact that the  $\text{VO}_4^{3-}$  group shows pronounced thermal quenching at those temperatures. This was studied in a diluted system with the same crystal structure, viz.  $\text{YP}_{0.95}\text{V}_{0.05}\text{O}_4$  [31].

A problem with this phosphor is that without precautions it usually contains a small amount of unreacted  $\text{V}_2\text{O}_5$  which lowers the light output. For application in high-pressure mercury vapor lamps this phosphor is usually prepared with an excess of boric acid. The material has then a white body color and, in addition, the particle size can be controlled. The boron is not built into the lattice; in some way or another the boron compound acts as a flux.

#### 6.4.4 Phosphors with Two-Photon Emission

All phosphors discussed up till now yield at best one visible photon for every absorbed ultraviolet photon. Taking the energy of short-wavelength radiation as about  $40\,000\text{ cm}^{-1}$ , and that of “average” visible light (500 nm) as  $20\,000\text{ cm}^{-1}$ , we lose about half of the energy. This energy is given up as heat to the host lattice in the several relaxation processes (Chapters 2 and 3); it is not a nonradiative transition which competes with the radiative one (Chapter 4).

A much higher energy efficiency can be obtained if the absorbed ultraviolet photon would split into two visible photons. Such a process would, in principle, have a quantum efficiency of 200%.

Two-photon emission has been reported for  $\text{Pr}^{3+}$  ( $4f^2$ ) in  $\text{YF}_3$  [32,33] with a quantum efficiency of about 145%. The energy level scheme is given in Fig. 6.23. The  $\text{Pr}^{3+}$  ion decays in two steps as indicated. The  $^1\text{S}_0$  level is at  $46\,500\text{ cm}^{-1}$ , and the  $^3\text{H}_4 \rightarrow ^1\text{S}_0$  transition parity forbidden. Excitation in a lamp has to occur in the  $4f^{5d}$  configuration of  $\text{Pr}^{3+}$  which is above the  $^1\text{S}_0$  level. Therefore the low-pressure mercury discharge cannot be applied and another solution has to be found.

Although two-photon emission would greatly enhance the efficiency of luminescent lamps, this concept has, up till now, found no practical realisation for lack of suitable materials and ultraviolet sources.

### 6.5 Outlook

It will be clear from this chapter that the introduction of rare-earth activated luminescent materials has drastically changed the situation. Apart from the cheaper halophosphate phosphors, we have now available a family of rare-earth activated phosphors which make luminescent lighting ideal. Not only the light output is high, but also the color rendering is excellent. For even better color rendering, the special deluxe lamps give a very good solution, although the light output is lower. The maintenance of these tricolor lamps is also very good. It is not realistic to anticipate important breakthroughs in this field.

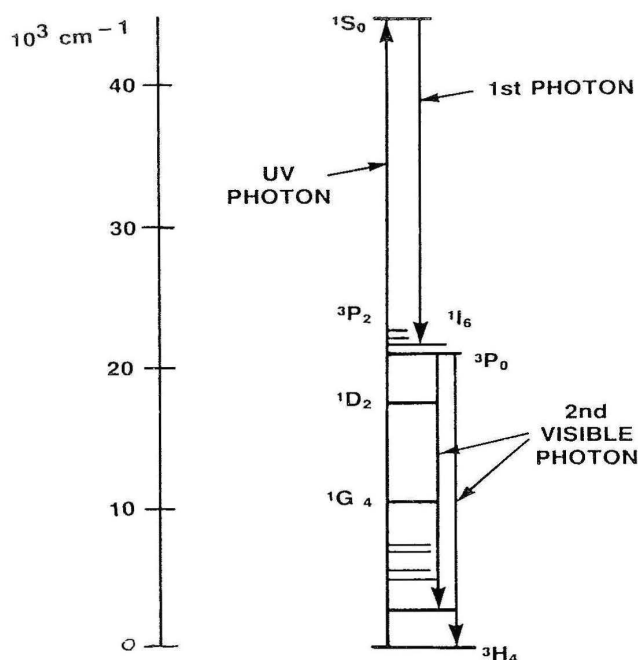


Fig. 6.23. Two-photon emission in  $\text{Pr}^{3+}$

It is therefore to be expected that the efforts of the lamp industry will go into the following directions:

- reduction of phosphor cost
- recovery of lamps in connection with (future) environmental requirements.

As a cheaper green the composition  $\text{Sr}_3\text{Gd}_2\text{Si}_6\text{O}_{18}:\text{Pb}^{2+}, \text{Mn}^{2+}$  has been suggested. However, this phosphor suffers from radiation damage [6]. A fundamental study has been devoted to the possibility of a cheaper red phosphor by activating calcium and zirconium compounds with  $\text{Eu}^{3+}$  [34,35]. In these hosts the  $\text{Eu}^{3+}$  ion carries an effective charge:  $\text{Eu}_{\text{Ca}}^{\bullet}$  or  $\text{Eu}_{\text{Zr}}'$ . The positive effective charge is detrimental for the quantum efficiency of the  $\text{Eu}^{3+}$  emission upon charge-transfer excitation ( $q_{\text{CT}}$ ), the negative effective charge is favorable. A qualitative model based on the configurational coordinate diagram has been proposed in order to explain these results. If the  $\text{Eu}^{3+}$  ion has a positive effective charge, the ground state shrinks more than the excited charge-transfer state, so that the value of  $q_{\text{CT}}$  decreases relative to that of  $\text{Y}_2\text{O}_3:\text{Eu}^{3+}$  (see Fig. 6.24). The only way to overcome this effect is to create very stiff surroundings around the  $\text{Eu}^{3+}$  ion. In this way  $q_{\text{CT}}$  values higher than 60% have been obtained.

For the negative effective charge more promising effects are to be expected and these have in fact been observed. Some  $\text{Eu}^{3+}$  ions in  $\text{BaZrO}_3:\text{Eu}^{3+}$  have a  $q_{\text{CT}}$  close to 100%. However, other  $\text{Eu}^{3+}$  ions have a much lower  $q_{\text{CT}}$ . Although it has become clear that cheaper lamp phosphors are not easy to find, this is not impossible in itself.

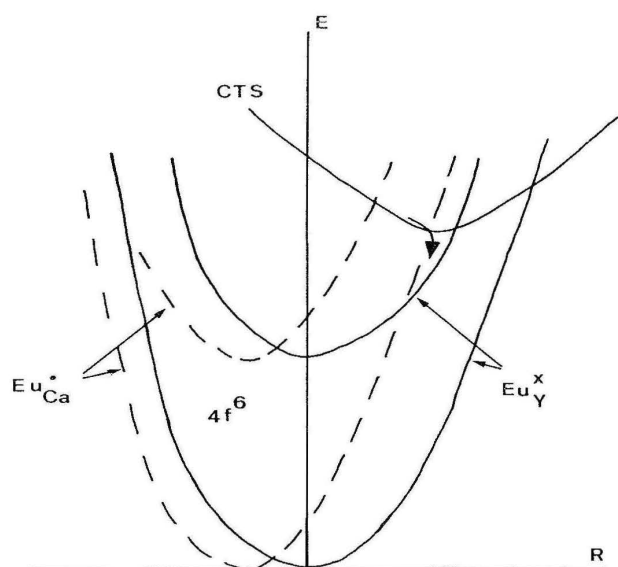


**Fig. 6.24.** Schematic configurational coordinate diagram for  $\text{Eu}^{3+}$  in oxides. Continuous lines relate to  $\text{Eu}^{3+}$  in an yttrium compound (e.g.  $\text{Eu}_Y^x$  in  $\text{Y}_2\text{O}_3:\text{Eu}^{3+}$ ). Broken lines relate to  $\text{Eu}^{3+}$  in a calcium compound (e.g.  $\text{Eu}_{\text{Ca}}^*$  in  $\text{CaSO}_4:\text{Eu}^{3+}$ ). The charge-transfer state is indicated by *CTS*. This state populates the emitting level in the case of  $\text{Eu}_Y^x$ , but the ground level in the case of  $\text{Eu}_{\text{Ca}}^*$ . See also text

Another trend in luminescent lamp research is the extension of the measurement of excitation spectra into the vacuum ultraviolet (see for example Ref. [36]). This has nowadays become feasible by using the possibilities of a synchrotron facility. High-energy excitation can also result in quantum efficiencies above 1. For example,  $\text{Y}_2\text{O}_3:\text{Eu}^{3+}$  shows a quantum efficiency of about 100% for 6 eV excitation, and 200% for 17 eV. This value increases to 240% for 23 eV [36]. These high values were ascribed to an interband Auger process. This implies the following: upon excitation, an electron from the valence band is brought high into the conduction band. The excess energy is used to excite another electron from the valence band into the conduction band, so that one exciting photon gives two (or more) electron-hole pairs which can recombine on the luminescent center. A knowledge of the excitation spectrum over a wide energy range is useful if one looks for other possibilities than mercury for the vapor discharge in the lamp.

For more specialized applications it might be that new phosphors are still to be found. Here we draw attention to a complete different application of photoluminescence proposed recently, viz. the use of ultraviolet headlights on cars in combination with luminescent marking of all road signs [37]. Experiments have shown that ultraviolet light can double the field of vision when compared with normal dipped lights. The introduction of this system seems to be simple and promises a higher road safety and even considerable cost savings. Other applications of this method were mentioned in the original report [37].

## References

1. Ouweltjes JL (1965) *Modern Materials*, vol 5, Academic, New York, p 161
2. Butler KH (1980) *Fluorescent lamp phosphors*, The Pennsylvania State University Press, University Park
3. Smets BMJ (1987) *Mat Chem Phys* 16:283; (1991) In: DiBartolo B (ed) *Advances in nonradiative processes in solids*, Plenum, New York, p 353; (1992) In: DiBartolo B (ed) *Optical properties of excited states in solids*, Plenum, New York, p 349
4. See e.g. West AR (1984) *Solid state chemistry and its applications*, Wiley, New York, Chapter 2
5. Maestro P, Huguenin D, Seigneurin A, Deneuve F, Le Lann P, Berar JF (1992) *J Electrochem Soc* 139:1479
6. Verhaar HCG, van Kemenade WMP (1992) *Mat Chem Phys* 31:213
7. Bailar Jr JC, Emeleus HJ, Nyholm R, Trotman-Dickenson AF (eds) (1973) *Comprehensive Inorganic Chemistry*, vol 1, p 540, Pergamon, Oxford
8. See e.g. Soules TF, Bateman RL, Hewes RA, Kreidler ER (1973) *Phys. Rev. B* 7 1657
9. Kröger FA (1973) *The chemistry of imperfect crystals*, 2nd edition, North-Holland, Amsterdam
10. Mishra KC, Patton RJ, Dale EA, Das TP (1987) *Phys. Rev. B* 35 1512
11. Oomen EWJL, Smit WMA, Blasse G (1988) *Mat Chem Phys* 19:357
12. Jenkins HG, McKeag AH, Ranby PN (1949) *J Electrochem Soc* 96:1
13. Versteegen JMPJ, Radielovic D, Vrenken LE (1974) *J Electrochem Soc* 121:1627
14. Koedam M, Opstelten JJ (1971) *Lighting Res. Technol.* 3:205
15. Buijs M, Meijerink A, Blasse G (1987) *J Luminescence* 37:9
16. van Schaik W, Blasse G (1992) *Chem Mater* 4:410
17. Smets BMJ, Verlijsdonk JG (1986) *Mat Res Bull* 21:1305; Ronda CR, Smets BMJ (1989) *J Electrochem Soc* 136:570
18. Smets BMJ, Rutten J, Hoeks G, Verlijsdonk J (1989) *J Electrochem Soc* 136:2119
19. Saubat B, Vlasse M, Fouassier C (1980) *J Solid State Chem* 34:271
20. Versteegen JMPJ, Sommerdijk JL, Verriet JG (1973) *J Luminescence* 6:425
21. van Schaik W, Lizzo S, Smit W, Blasse G (1993) *J Electrochem Soc* 140:216
22. Blasse G (1988) *Progress Solid State Chemistry* 18:79
23. van Schaik W, Blasse G, to be published
24. Blasse G (1986) *J Solid State Chem* 62:207
25. Atkins PW (1990) *Physical Chemistry*, 4th ed Oxford University, Oxford
26. Blasse G (1992) *Int Revs Phys Chem* 11:71
27. Blasse G, de Korte PHM (1981) *J Inorg Nucl Chem* 43:1505
28. Donker H, Smit WMA, Blasse G (1989) *J Electrochem Soc* 136:3130
29. Levine AK, Palilla FC (1964) *Appl Phys Letters* 5:118
30. Wanmaker WL, ter Vrugt JW (1971) *Lighting Res Technol* 3:147
31. Blasse G (1968) *Philips Res Repts* 23:344
32. Sommerdijk JL, Bril A, de Jager AW (1974) *J Luminescence* 8:341
33. Piper WW, de Luca JA, Ham FS (1974) *J Luminescence* 8:344
34. van der Voort D, Blasse G (1991) *Chem Mater* 3:1041
35. Alarcon J, van der Voort D, Blasse G (1992) *Mat Res Bull* 27:467
36. Berkowitz JK, Olsen JA (1991) *J Luminescence* 50:111
37. Bergkvist L, Bringfeldt G, Fast P, Granstrom U, Ilhage B, Kallioniemi C (1990) *Volvo Technology Report*, p 44
38. Struck CW, Fonger WH (1970) *J Luminescence* 1,2:456

## CHAPTER 7

# Cathode-Ray Phosphors

### 7.1 Cathode-Ray Tubes: Principles and Display

Devices in which phosphors are excited by means of cathode rays have great practical importance: cathode-ray tubes are used for television, oscilloscopes, electron microscopes, etc. Cathode rays are a beam of fast electrons; the accelerating voltage in a television picture tube is high ( $> 10$  kV). Figure 7.1 presents a schematic picture of such a tube. The electron beam can be deflected by a magnetic field.

In a color television tube the luminescent screen consists of a regular array of three kinds of phosphor dots: red-emitting dots, green-emitting dots and blue-emitting dots. There is an electron gun for the red dots giving a red picture, a gun for the green dots and one for the blue dots.

As we have seen in Sect. 6.2, additive mixing of primary colors in the form of blue, green and red phosphor emissions allows the production of all colors within the triangle enclosed in the chromaticity diagram (Fig. 7.2). For black-and-white television a bluish-white emission color is preferred. This can be obtained by several

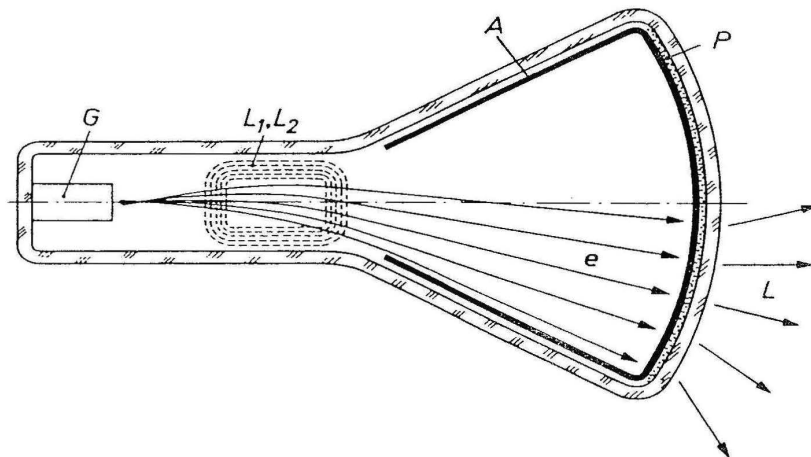


**Fig. 7.1.** Principle of the cathode-ray tube. Electrons ( $e$ ) leaving the electron gun ( $G$ ) are deflected by the systems  $L_1$ ,  $L_2$ , and excite the luminescent material  $P$ .  $A$  is the anode and  $L$  the emitted radiation



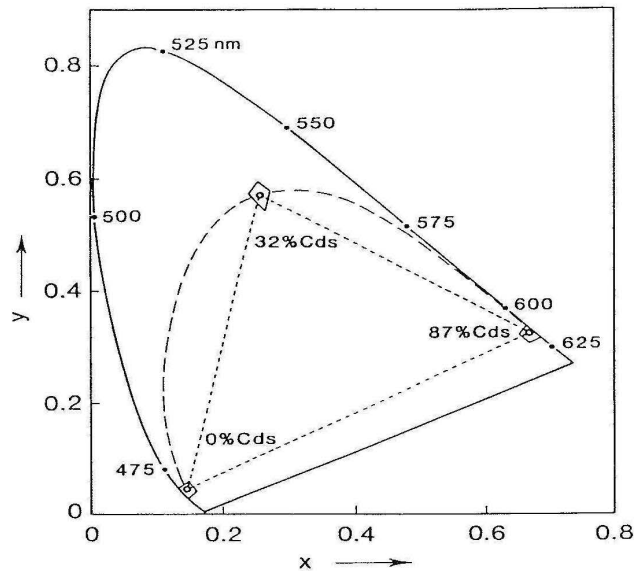


**Fig. 7.2.** CIE chromaticity diagram. The solid curve indicates monochromatic radiation marked by its wavelength in nm. The small quadrilaterals correspond with internationally agreed tolerance ranges. See also text

mixtures of two phosphors. In color television the problem is more complicated. The three phosphors have to be selected in such a way that the brightness is high and colors are well reproduced. Note that this is a problem different from that in lighting, where the color reproduction of illuminated objects is essential (Sect. 6.2).

Although great progress in other display techniques has been made in recent years, for example liquid crystal and electroluminescent panels, the properties of the cathode-ray tube remain up till now unsurpassed. This can be attributed to several factors. Among these are the high radiant efficiency of modern cathode-ray phosphors, their high brightness, their long life time in the tube, and the ease with which large-area uniform layers can be deposited.

Since we are dealing with a vacuum tube, the upper limit of the screen which can be reached by present-day technology is about 75 cm. Pictures with a 2 m diameter can be obtained in projection television (PTV). For each of the three colors a small (monochrome) cathode-ray tube is used. Their images are optically projected and superimposed on a projection screen using a lens system. In such a way a composite picture in full color is shown on the screen (Fig. 7.3). In order to obtain high illumination levels on the large screen, much higher current densities have to be used in PTV than in direct-view cathode-ray tubes.

Unfortunately the luminescence output is no longer linearly proportional with current density for high excitation densities (as it is for low excitation densities). Saturation occurs. Actually it is hard to find materials which satisfy all the requirements, as we will see later (see below).